A smoothness indicators free third-order weighted ENO scheme for gas-dynamic Euler equations

Shujiang Tang (sjtang@xtu.edu.cn)
School of Mathematics and Computational Science, Xiangtan University

Research Article

Keywords: WENO scheme, high efficiency, high resolution, smoothness indicators free, low consumption

Posted Date: June 9th, 2022

DOI: https://doi.org/10.21203/rs.3.rs-1720961/v1

A smoothness indicators free third-order weighted ENO scheme for gas-dynamic Euler equations

Shujiang Tang*[a,b]

[a] School of Mathematics and Computational Science, Xiangtan University, Hunan, 411105, China
[b] Hunan Key Laboratory for Computation and Simulation in Science and Engineering, Xiangtan University, Hunan, 411105, China

Abstract

To improve the shock-capturing capability of the third-order WENO scheme and enhance its computational efficiency, in this paper, we designed a new WENO scheme independent of the local smooth factor, WENO-SIF. The weight functions of the WENO-SIF scheme are segmentation functions of the sub-stencils, which can guarantee it achieves the desired accuracy at the high-order critical points. During the calculation, WENO-SIF need not calculate the smoothing factor, which can effectively reduce the computational consumption. The new WENO-SIF is compared with WENO-JS and other WENO schemes for numerical experiments at one- and two-dimensional benchmark problems with a suitable choice of $\lambda = 0.13$. The results show the WENO scheme can further improve the resolution of WENO-JS, achieve the optimal accuracy at high-order critical points, and significantly reduce computational consumption.

Keywords: WENO scheme, high efficiency, high resolution, smoothness indicators free, low consumption

1. Introduction

Based on the ENO scheme [1], Liu et al. [2] proposed the WENO method that can maintain the ENO property in the smooth region by recombining the sub-templates using a weighting function. Because of the high accuracy and the essentially oscillatory of the WENO scheme, it has been widely used and vigorously developed in fluid mechanics and aerospace. Jiang and Shu [3] proposed a technique that can measure the smoothness of sub-templates, and they gave a framework for building the WENO method with various accuracies. Since then, the researchers have conducted tests, evaluations, and improvements on the WENO method [4, 5, 6, 7].

Henrick et al. [8] found that the fifth-order WENO-JS scheme suffers from accuracy degradation at the extremum. And they developed a mapping function, which resulted in a fifth-order accuracy WENO-M method that can achieve the best at the first-order critical point. Since then, Feng [9, 10], Wang [11], Vevek [12], Hong [13], Hu [14], Li [15, 16], Zhu [17] have developed a series of mapping functions successively to develop different higher-order mapping type WENO schemes. Unlike Henrick's mapping-type WENO scheme, Borges et al. [18] designed a new type of nonlinear weights by using a linear combination of low-order local smoothness factors to construct a global high-order smoothness factor. And they developed a class of structurally simple fifth-order WENO-Z schemes. In addition, Castro [19], Don [20], Liu [21], Wang [22], Peng [23], Mulet [24, 25, 26], Hu [27], Russo [28, 29, 30], Rathan [31] and Huang [32] have successively developed various high order WENO-Z type schemes based on Borges'.

*Corresponding author
Email address: sjtang@xtu.edu.cn (Shujiang Tang*)

Compared with higher-order WENO schemes of fifth-order and above, the third-order WENO scheme is more robust in capturing shocks, uses fewer grid points, and can be easily extended to unstructured grids. However, it also suffers from shortcomings, such as higher dissipation and lower accuracy. Yamaleev et al. [33] developed a high-resolution third-order energy-stable WENO scheme (ESWENO) using an amount-preserving stable global smoothness factor. Liu et al. [34] proposed the WENO-MN scheme using the values of all three points on the global stencil of the third-order WENO scheme to calculate the local smoothness factor. Wu et al.[35, 36, 37] developed three WENO schemes, namely WENO-N, WENO-NP, and WENO-NN, using different nonlinear combinations of local smoothness indicators and local smoothness factors. Wang et al. [38] introduced a new reference smoothness indicator to construct a third-order WENO-R scheme with low dissipation. Li et al. [39] constructed a new global smoothness indicator by using Taylor expansions to handle local smoothness indicators and developed the WENO-ZF scheme. Li et al.[40] designed two new global smoothness indicators by non-linearly combining local smoothness indicators with reference values based on Lagrangian interpolation polynomials and developed the WENO-L3 and WENO-L4. Tang et al. [41] constructed three multi-parameter types finite volume WENO schemes by modifying the weight functions of the WENO scheme using the construction of the limiter of the MUSCL scheme. In addition, many other scholars have improved the third-order WENO scheme and developed many new schemes.[42, 43, 44]

However, the various current third-order WENO schemes suffer from two shortcomings: First, they cannot achieve optimal accuracy at high-order critical points. Second, some high-resolution WENO schemes suffer from relatively complicated construction of the weight function and low computational efficiency. To address these problems, in this paper, we improve the WENO scheme by constructing a weight function that does not depend on the local smooth factor. The results of WENO-SIF show it can achieve optimal weights at higher-order critical points and has a simple and efficient structure. The present WENO-SIF scheme with $\lambda = 0.13$ has better spectral properties and higher resolution through ADR analysis [45] and calculation of various 1D-2D problems, and its computational efficiency is much higher than other given WENO schemes.

We set the basic framework for this paper: Section 2 presents the structure of classical third-order WENO schemes. In Section 3, we give construction tips for the new WENO scheme and determine the parameters of the weight function in the new scheme by using the ADR method. In Section 4, we compare the performance of various WENO schemes in terms of accuracy at higher-order critical points, resolution, and computational efficiency for 1-D and 2-D Euler gas dynamics. We will provide the conclusions of this paper in Section 5.

2. Reviews of WENO methods

In this section, we briefly introduce a series of third-order WENO schemes. Consider the following one-dimensional scalar hyperbolic conservation laws.

$$\begin{cases} u_t + f(u)_x = 0, \\ u(x,0) = u_0(x). \end{cases} \tag{1}$$

Discretizing the computational region as a uniform interval of Δx yields a conservative scheme of semi-differentiation of the following form:

$$\frac{du_j}{dt} = -\frac{1}{\Delta x}(\hat{f}_{j+1/2} - \hat{f}_{j-1/2}), \tag{2}$$

where $\hat{f}_{j+1/2} = \hat{f}^+_{j+1/2} + \hat{f}^-_{j+1/2}$ is the numerical flux, which satisfies $df^+(u)/du \geq 0$ and $df^-(u)/du \leq 0$. Since $\hat{f}^+_{j+1/2}$ and $\hat{f}^-_{j+1/2}$ are approximated similarly, for convenience, we will only describe the approximation of $\hat{f}^+_{j+1/2}$. For simplicity,

we will remove the superscript $+$ of the flux.

On the 3-point stencil at the central node $x_{j-1/2}$, the numerical flux function of the third-order finite-difference WENO scheme is defined as:

$$\hat{f}_{j+1/2} = \omega_0 q_0 + \omega_1 q_1, \tag{3}$$

where q_k is the second-order flux on the sub-stencil $S_k = \{j-1+k, j+k\},\ k = 0, 1$, which is defined by

$$\begin{cases} q_0 = (-f_{j-1} + 3f_j)/2, \\ q_1 = (f_j + f_{j+1})/2. \end{cases} \tag{4}$$

And the weights ω_k will be introduced in the following subsections.

2.1. WENO-JS scheme

The nonlinear weights proposed by Jiang and Shu [3] are

$$\omega_k^{JS} = \frac{\alpha_k}{\alpha_0 + \alpha_1}, \alpha_k = \frac{d_k}{(\beta_k + \epsilon)^2},\ k = 0, 1, \tag{5}$$

where $(d_0,\ d_1) = (1/3,\ 2/3)$. ϵ is a positive number with the value 10^{-6} to avoid the denominator becoming zero in the smoothing region. The local smoothness indicators β_k in the stencils are calculated by

$$\beta_k = \sum_{m=1}^{r-1} \triangle x^{2m-1} \int_{x_{j-1/2}}^{x_{j+1/2}} \left(\frac{d^m \widehat{f}_k}{dx^m} \right)^2 dx, \tag{6}$$

where $r = 2$ is the number of sub-stencils. And the local smoothness indicators of the third-order WENO scheme are

$$\begin{cases} \beta_0 = (f_j - f_{j-1})^2, \\ \beta_1 = (f_{j+1} - f_j)^2. \end{cases} \tag{7}$$

Taylor expansion of Eq. (7) at the point x_j yields

$$\begin{cases} \beta_0 = f_j'^2(\Delta x)^2 - f_j' f_j''(\Delta x)^3 + \left(\frac{1}{3} f_j' f_j''' + \frac{1}{4} f_j''^2\right)(\Delta x)^4 - \left(\frac{1}{12} f_j' f_j^{(4)} + \frac{1}{6} f_j'' f_j'''\right)(\Delta x)^5 + O(\Delta x^6), \\ \beta_1 = f_j'^2(\Delta x)^2 + f_j' f_j''(\Delta x)^3 + \left(\frac{1}{3} f_j' f_j''' + \frac{1}{4} f_j''^2\right)(\Delta x)^4 + \left(\frac{1}{12} f_j' f_j^{(4)} + \frac{1}{6} f_j'' f_j'''\right)(\Delta x)^5 + O(\Delta x^6). \end{cases} \tag{8}$$

Easy to verify that

$$\beta_k = (\Delta x)^{2(n_{cp}+1)}(1 + O(\Delta x)),\ k = 0, 1, \tag{9}$$

where n_{cp} is a integer that satisfies the following condition: if the function $f(x)$ has $n_{cp}+1$-order derivatives and satisfies, $f'(x_0) = f''(x_0) = \cdots = f^{(n_{cp})}(x_0) = 0$, and $f^{(n_{cp}+1)}(x_0) \neq 0$, then x_0 is said to be a n_{cp}-order critical point of the function $f(x)$.

Substituting (9) into (5) and ignoring ϵ, we get

$$\omega_k = \begin{cases} d_k(1 + O(\Delta x)^2), & n_{cp} = 0, \\ d_k(1 + O(\Delta x)), & n_{cp} \geq 1. \end{cases} \tag{10}$$

To get high accuracy numerical solution, the nonlinear weights of the WENO scheme should be approximately equal to the linear at the smooth region. Yamaleev et al. [33] proposed a sufficient condition for the third-order accuracy of the weights ω_k

$$\omega_k = d_k(1 + O(\Delta x)^2), \tag{11}$$

It can be seen that WENO-JS will reduce the order at the high-order critical point.

2.2. WENO-Z-type scheme

To improve the accuracy of WENO-JS, Borges et al. [18] constructed a fifth-order WENO-Z scheme capable of achieving the optimal accuracy at the first-order critical point by introducing a global smoothness indicator. Similar to the fifth-order WENO-Z scheme, the weights of the third-order WENO-Z-type scheme are calculate as following

$$\tau_3 = |\beta_1 - \beta_0| . \tag{12}$$

From this, the weight functions of the third-order WENO-Z scheme can be got as:

$$\omega_k^Z = \frac{\alpha_k^Z}{\sum_{i=0}^{1} \alpha_i^Z}, \alpha_k^Z = d_k \left(1 + \frac{\tau_3}{\beta_k + \epsilon}\right), \ k = 0, 1, \tag{13}$$

In the smooth region, the Taylor expansion of equation (13) at the point x_j gives

$$\begin{aligned} \tau_3 &= \left| 2 f_j' f_j''' (\Delta x)^3 + \left(\frac{1}{6} f_j' f_j^{(4)} + \frac{1}{3} f_j'' f_j'''\right) (\Delta x)^5 + \left(\frac{1}{360} f_j' f_j^{(6)} + \frac{1}{120} f_j'' f_j^{(5)} + \frac{1}{72} f_j''' f_j^{(4)}\right) (\Delta x)^7 + O(\Delta x^9) \right| \\ &= (\Delta x)^{2(n_{cp}+1)+1}. \end{aligned} \tag{14}$$

Thus

$$\omega_k^Z = d_k(1 + O(\Delta x)), \quad k = 0, 1. \tag{15}$$

From equation (15), one can see that the weight function in WENO-Z scheme does not satisfy the sufficient conditions given by Yamaleev et al. However, the numerical results show that the WENO-Z can achieve the optimal accuracy at the 0th order critical point.

Xu et al. [37] proposed a new WENO-Z type scheme, WENO-PZ, by slightly modifying the local smoothness indicator of the third-order WENO-Z by using Taylor expansion. And they gave the following new reference smoothness indicator

$$\omega_k^{PZ} = \frac{\alpha_k^Z}{\sum_{i=0}^{1} \alpha_i^Z}, \alpha_k^Z = d_k \left(1 + \frac{\tau_3}{(\beta_k + \epsilon)^p}\right), \ k = 0, 1, \tag{16}$$

To enable the WENO-PZ scheme to achieve high accuracy at the critical points, Xu et al. set the value of p to $3/4$. However, since the exponents of the local-smooth factors in WENO-PZ are rational numbers, they consume a lot of computational time during the calculation, a conclusion we will give later in the numerical calculation section.

2.3. WENO-M scheme

To overcome the fifith-order WENO-JS scheme will lose accuracy at the critical points, Henrick et al. [8] designed the following mapping function to improve the approximation accuracy of ω_k^{JS}

$$g(\omega_k^{JS}) = \frac{\omega_k^{JS}(d_k + d_k^2 - 3d_k\omega_k^{JS} + (\omega_k^{JS})^2)}{d_k^2 + \omega_k^{JS}(1 - 2d_k)}, \ k = 0, 1. \tag{17}$$

Similar to the fifth-order WENO-M scheme, the weights of the third-order WENO-M-type are as follows

$$\omega_k^M = \frac{g(\omega_k^{JS})}{g(\omega_0^{JS}) + g(\omega_1^{JS})}, \ k = 0, 1, 2. \tag{18}$$

A Taylor expansion of equation (17) at d_k gives

$$g(\omega_k^{JS}) = d_k(+O((\Delta x)^3)). \tag{19}$$

Thus

$$\omega_k^M = d_k(+O((\Delta x)^3)), \tag{20}$$

that is, the WENO-M satisfies the sufficient condition for the third-order accuracy of the weights. Interestingly, although WENO-M can achieve theoretically the optimal accuracy, it is not computationally achievable. This conclusion we will present in the section on numerical calculations.

2.4. WENO-MN scheme

Liu et al. [34] constructed a new class of local smoothness factors by approximating the first-order derivatives of the flux f at the nodes $j-1, j$ and $j+1$.

$$\begin{cases} \beta_0^{MN} = \frac{1}{4}(|f_{j+1} - f_{j-1}| - |f_{j+1} - 4f_j + 3f_{j-1}|)^2, \\ \beta_1^{MN} = \frac{1}{4}(|f_{j+1} - f_{j-1}| - |3f_{j+1} - 4f_j + f_{j-1}|)^2. \end{cases} \tag{21}$$

In the smooth region, the Taylor series expansions of (21) are

$$\begin{cases} \beta_0^{MN} = \left(\left|f_j'\Delta x + \frac{1}{6}f_j'''(\Delta x)^3 + O(\Delta x)^5\right| - \left|f_j'\Delta x - f_j''(\Delta x)^2 + \frac{1}{6}f_j'''(\Delta x)^3 - \frac{1}{12}f_j^{(4)}(\Delta x)^4 + O(\Delta x)^5\right|\right)^2, \\ \beta_1^{MN} = \left(\left|f_j'\Delta x + \frac{1}{6}f_j'''(\Delta x)^3 + O(\Delta x)^5\right| - \left|f_j'\Delta x + f_j''(\Delta x)^2 + \frac{1}{6}f_j'''(\Delta x)^3 + \frac{1}{12}f_j^{(4)}(\Delta x)^4 + O(\Delta x)^5\right|\right)^2. \end{cases} \tag{22}$$

Thus, the weights of the WENO-JS-type scheme WENO-MN satisfies

$$\omega_k^{MN} = \frac{d_k/(\beta_k^{MN} + \epsilon)^2}{d_0/(\beta_0^{MN} + \epsilon)^2 + d_1/(\beta_1^{MN} + \epsilon)^2} = d_k(1 + O((\Delta x))),\ k = 0, 1. \tag{23}$$

Liu et al. pointed out that the weights of the WENO-MN scheme do not meet the sufficient condition near the critical point, and its numerical dissipation will be significantly smaller than that of the WENO-JS in the smooth region.

3. Design and properties of the new WENO scheme

In this section, we propose a new WENO scheme independent of the local smoothing factor. The specific construction process of WENO-SIF is divided into the following parts.

First, we reconstruct the weight functions of WENO-JS. It may be assumed that

$$r_j = \frac{|f_j - f_{j-1}| + \epsilon}{|f_{j+1} - f_j| + \epsilon}, \tag{24}$$

where ϵ is a positive number to prevent the numerator and denominator from being equal to zero, and in this paper, we always take the value $\epsilon = 10^{-40}$ without specifical specification. Thus, the weight functions of WENO-JS can always be rewritten in the following form

$$\omega_0^{JS} = \frac{1}{1 + 2r_j^4},\ \omega_1^{JS} = \frac{2r_j^4}{1 + 2r_j^4}. \tag{25}$$

Similarly, the weight functions of the WENO-Z scheme can be rewritten as

$$\omega_0^Z = \frac{r_j^2 + \left|1 - r_j^2\right|}{3r_j^2 + (1 + 2r_j^2)\left|1 - r_j^2\right|},\ \omega_1^Z = \frac{2r_j^2(1 + \left|1 - r_j^2\right|)}{3r_j^2 + (1 + 2r_j^2)\left|1 - r_j^2\right|}. \tag{26}$$

In contrast, the weight functions of the WENO-MN scheme can be rewritten as

$$\omega_0^{MN} = \frac{(|1 + r_j| - |3 - r_j|)^2}{(|1 + r_j| - |3 - r_j|)^2 + 2(|1 + r_j| - |1 - 3r_j|)^2},\ \omega_1^{MN} = \frac{2(|1 + r_j| - |1 - 3r_j|)^2}{(|1 + r_j| - |3 - r_j|)^2 + 2(|1 + r_j| - |1 - 3r_j|)^2}. \tag{27}$$

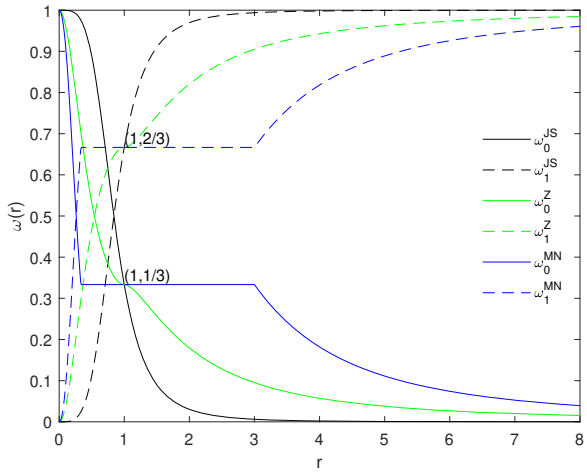

Fig. 1: Curves of weight functions of WENO-JS(black), WENO-Z(green) and WENO-MN(blue).

Figure 1 represents the weight function curves of WENO-JS, WENO-Z and WENO-MN. One can see that ω_0^{JS}, ω_0^Z and ω_0^{MN} are monotonically decreasing with r and all pass through the point $(1, 1/3)$. And ω_1^{JS}, ω_1^Z and ω_1^{MN} are monotonically increasing with respect to r and all pass through the point $(1, 2/3)$.

Second, combining the characteristics of the above several WENO schemes, we can always construct various improved WENO schemes without local smooth factors that satisfy the third-order condition by using functions of r_j. That leads to a conclusion as follows.

Theorem 1 If the weight functions $\omega_k(r_j),\ k = 0, 1$ satisfies the following conditions:

(a) $\omega_0(r_j)$ (or $\omega_1(r_j)$) is monotone decrease (or increase) with r_j, and satisying $\omega_0(0) = 1$ (or $\omega_1(0) = 0$), $\omega_0(1) = 1/3$ (or $\omega_1(1) = 2/3$) and $\omega_0(\infty) = 0$ (or $\omega_1(\infty) = 1$).

(b) The point $r_j = 1$ is the 2nd-order critical point of the function $\omega_k(r_j),\ k = 0, 1$.

Then, the resulting WENO scheme can achieve optimal accuracy at any critical point.

Proof Ignoring ϵ in equation (24), we get

$$\begin{aligned} r_j &= \frac{\left|f_j - \left(f_j - f_j'\Delta x + \frac{1}{2!}f_j''(\Delta x)^2 - \frac{1}{3!}f_j'''(\Delta x)^3 + O((\Delta x)^4)\right)\right|}{\left|\left(f_j + f_j'\Delta x + \frac{1}{2!}f_j''(\Delta x)^2 + \frac{1}{3!}f_j'''(\Delta x)^3 + O((\Delta x)^4)\right) - f_j\right|} \\ &= \frac{\left|f_j'\Delta x - \frac{1}{2!}f_j''(\Delta x)^2 + \frac{1}{3!}f_j'''(\Delta x)^3 + O((\Delta x)^4)\right|}{\left|f_j'\Delta x + \frac{1}{2!}f_j''(\Delta x)^2 + \frac{1}{3!}f_j'''(\Delta x)^3 + O((\Delta x)^4)\right|} \\ &= 1 + O(\Delta x),\ n_{cp} \geq 0, \end{aligned} \tag{28}$$

Suppose that $\omega_k(r_j),\ k = 0, 1$ satisfies the two conditions in the theorem, then

$$\begin{aligned} \omega_k(r_j) &= \omega_k(1) + \omega_k'(1)(r_j - 1) + \frac{\omega_k''(1)}{2!}(r_j - 1)^2 + \frac{\omega_k'''(1)}{3!}(r_j - 1)^3 + O((r_j - 1)^4) \\ &= d_k + \frac{\omega_k'''(1)}{3!}(\Delta x)^3 + O((\Delta x)^4),\ k = 0, 1. \end{aligned} \tag{29}$$

These weight functions will satisfy the sufficient conditions for third-order accuracy at any-order critical point.

To reduce the consumption of the weight function in the calculation process and ensure that the new WENO scheme can achieve optimal accuracy at any critical point, we construct weight functions of the following form by combining the

two conditions in Theorem 1.

$$\begin{cases} \omega_0(r_j) = \begin{cases} 1, & r_j < \lambda, \\ 1/3, & \lambda \le r_j \le 1/\lambda, \\ 0, & otherwise, \end{cases} \\ \omega_1(r_j) = 1 - \omega_0(r_j), \end{cases} \tag{30}$$

in which, λ is a positive number less than 1 to be determined. We refer to the new WENO scheme equipped with the weight function of (30) as the local smooth factor-free WENO scheme, or WENO-SIF for short.

It is easy to verify that WENO-SIF satisfies all the conditions of Theorem 1 when $\lambda < 1$. And the value of λ will affect the numerical stability and resolution of the WENO-SIF scheme.

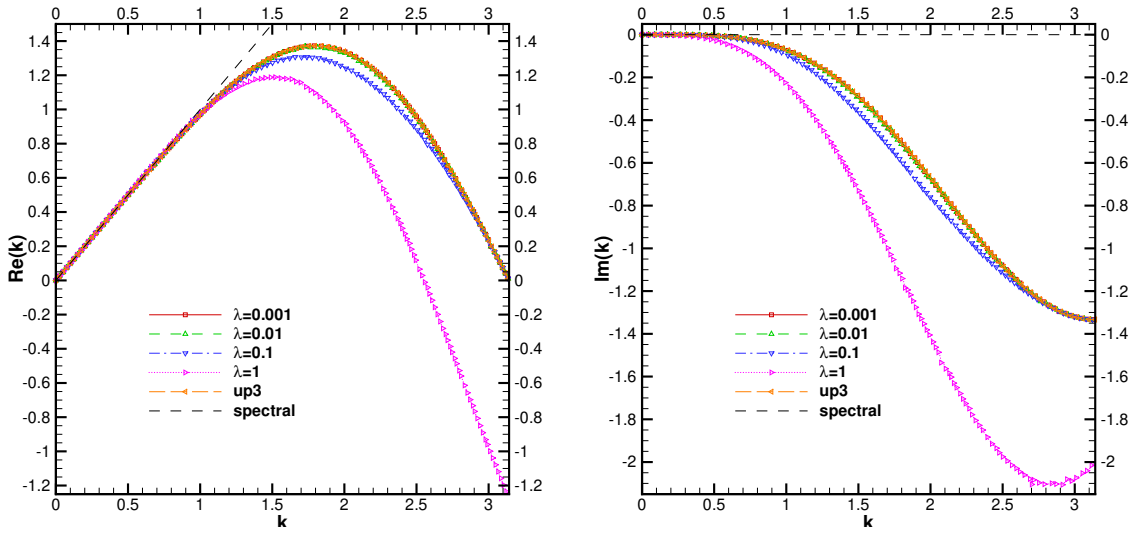

Fig. 2: Dispersion and dissipation curves of WENO-SIF with selected λ.

Figure 2 depicts the spectral properties of WENO-SIF by using the approximate dispersion relation of the shock capture method (ADR) [45]. It is easy to see that when $\lambda \to 0$, the spectrum of WENO-SIF is very close to the third-order linear upwind scheme. To make WENO-SIF with good numerical stability and high resolution, of thumb, in this paper, we will always choose $\lambda = 0.13$.

We also compared the dispersion and dispersion of the third-order WENO-JS, WENO-Z, WENO-M, WENO-PZ ($p = 3/4$), WENO-MN, WENO-SIF, and the third-order upwind scheme, and the results shown in Figure 3. From the figure, one can see that WENO-SIF has better spectral characteristics than other WENO schemes.

4. Numerical results

In this section, we will compare the performance of the present third-order WENO-SIF with WENO-JS, WENO-Z, WENO-M, WENO-PZ and WENO-MN by computing several classical problems, where the time advance is the third-order

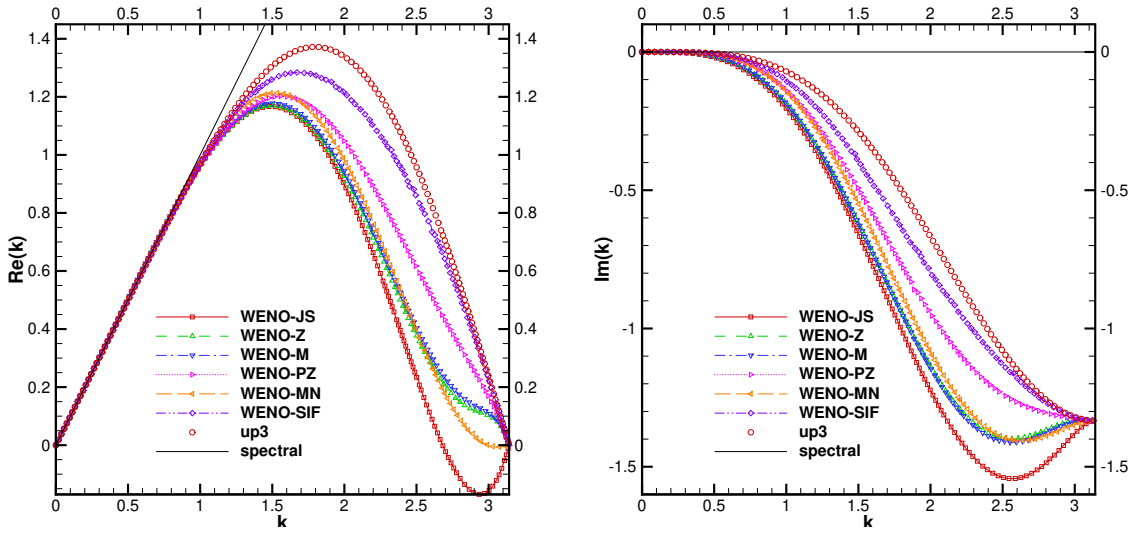

Fig. 3: Dispersion and dissipation curves of various WENO schemes.

TVD Runge-Kutta method [3].

$$
\begin{aligned}
u^{(1)} &= u^n + \triangle t^n C[u^n], \\
u^{(2)} &= \frac{3}{4}u^n + \frac{1}{4}(u^{(1)} + \triangle t^n C[u^{(1)}]), \\
u^{(3)} &= \frac{1}{3}u^n + \frac{2}{3}(u^{(2)} + \triangle t^n C[u^{(2)}]),
\end{aligned} \tag{31}
$$

where $C[u^n]$ denote the numerical flux. Without specified, we will set ϵ to be $1e-40$ in the following, except for WENO-JS ($\epsilon = 1e-6$), and the CFL number is 0.6. In the following, CPU times for all 1-D problems are the averaged values of 100 calculations run with an Intel i3-10100 @ 3.60GHz processor.

4.1. Convergence at higher-order critical points

In this subsection, we will compare various WENO schemes by computing the accuracy of a function at the critical points of the selected order. Given a trial function of the following form

$$
f(x) = e^x - \sum_{k=1}^{n_{cp}} \frac{x^k}{k!}. \tag{32}
$$

Then, the value of the kth order derivative of this function at the point $x_0 = 0$ is

$$
f^{(k)}(0) = \begin{cases} 0, & k \le n_{cp}, \\ 1, & otherwise, \end{cases} \tag{33}
$$

that is, $x_0 = 0$ is the n_{cp} order critical point of $f(x)$.

For each n_{cp}, we investigate the convergence of the critical point $x_0 = 0$ at six levels from $q = 0$ to 5. Where each level defined as $\triangle x = 0.001/2^q$. Tables 1-3 list the L^1, L^2 and L^∞ errors and convergence rates in the approximation of $f(x_{\frac{1}{2}}) - f(x_{-\frac{1}{2}})$.

Table 1: Convergence properites of various WENO schemes at $n_{cp} = 0$ critical point.

	q	L^1-error	L^1-order	L^2-error	L^2-order	L^∞-error	L^∞-order
WENO-JS	0	$0.45205e-07$		$0.45205e-07$		$0.45205e-07$	
	1	$0.28233e-08$	4.00	$0.39927e-08$	3.50	$0.56465e-08$	3.00
	2	$0.23519e-09$	3.59	$0.40735e-09$	3.30	$0.70556e-09$	3.00
	3	$0.22045e-10$	3.42	$0.44089e-10$	3.21	$0.88178e-10$	3.00
	4	$0.22043e-11$	3.32	$0.49289e-11$	3.16	$0.11021e-10$	3.00
	5	$0.22960e-12$	3.26	$0.56240e-12$	3.13	$0.13776e-11$	3.00
WENO-Z	0	$0.10122e-07$		$0.10122e-07$		$0.10122e-07$	
	1	$0.64176e-09$	3.98	$0.90759e-09$	3.48	$0.12835e-08$	2.98
	2	$0.53866e-10$	3.57	$0.93298e-10$	3.28	$0.16160e-09$	2.99
	3	$0.50681e-11$	3.41	$0.10136e-10$	3.20	$0.20272e-10$	2.99
	4	$0.50772e-12$	3.31	$0.11353e-11$	3.16	$0.25386e-11$	3.00
	5	$0.52934e-13$	3.26	$0.12966e-12$	3.13	$0.31761e-12$	3.00
WENO-M	0	$0.10391e-07$		$0.10391e-07$		$0.10391e-07$	
	1	$0.65031e-09$	4.00	$0.91968e-09$	3.50	$0.13006e-08$	3.00
	2	$0.54225e-10$	3.58	$0.93920e-10$	3.29	$0.16267e-09$	3.00
	3	$0.50850e-11$	3.41	$0.10170e-10$	3.21	$0.20340e-10$	3.00
	4	$0.50856e-12$	3.32	$0.11372e-11$	3.16	$0.25428e-11$	3.00
	5	$0.52979e-13$	3.26	$0.12977e-12$	3.13	$0.31787e-12$	3.00
WENO-PZ	0	$0.10374e-07$		$0.10374e-07$		$0.10374e-07$	
	1	$0.64990e-09$	4.00	$0.91910e-09$	3.50	$0.12998e-08$	3.00
	2	$0.54212e-10$	3.58	$0.93898e-10$	3.29	$0.16264e-09$	3.00
	3	$0.50845e-11$	3.41	$0.10169e-10$	3.21	$0.20338e-10$	3.00
	4	$0.50855e-12$	3.32	$0.11371e-11$	3.16	$0.25427e-11$	3.00
	5	$0.52978e-13$	3.26	$0.12977e-12$	3.13	$0.31787e-12$	3.00
WENO-MN	0	$0.10396e-07$		$0.10396e-07$		$0.10396e-07$	
	1	$0.65039e-09$	4.00	$0.91979e-09$	3.50	$0.13008e-08$	3.00
	2	$0.54226e-10$	3.58	$0.93923e-10$	3.29	$0.16268e-09$	3.00
	3	$0.50850e-11$	3.41	$0.10170e-10$	3.21	$0.20340e-10$	3.00
	4	$0.50856e-12$	3.32	$0.11372e-11$	3.16	$0.25428e-11$	3.00
	5	$0.52979e-13$	3.26	$0.12977e-12$	3.13	$0.31787e-12$	3.00
WENO-SIF	0	$0.10396e-07$		$0.10396e-07$		$0.10396e-07$	
	1	$0.65039e-09$	4.00	$0.91979e-09$	3.50	$0.13008e-08$	3.00
	2	$0.54226e-10$	3.58	$0.93923e-10$	3.29	$0.16268e-09$	3.00
	3	$0.50850e-11$	3.41	$0.10170e-10$	3.21	$0.20340e-10$	3.00
	4	$0.50856e-12$	3.32	$0.11372e-11$	3.16	$0.25428e-11$	3.00
	5	$0.52979e-13$	3.26	$0.12977e-12$	3.13	$0.31787e-12$	3.00

Table 1 shows all the computational errors and accuracies of various WENO schemes for the $n_{cp} = 0$ critical point $x_c = 0$. One can see that all the WENO schemes achieve third-order accuracy. The errors of WENO-Z, WENO-M, WENO-PZ, WENO-MN, and WENO-SIF are about the same and smaller than those of the WENO-JS scheme. That shows the WENO-SIF scheme can achieve optimal accuracy at the 0th-order critical point.

Table 2: Convergence properites of various WENO schemes at $n_{cp} = 1$ critical point.

	q	L^1-error	L^1-order	L^2-error	L^2-order	L^∞-error	L^∞-order
WENO-JS	0	$0.82120e-03$		$0.82120e-03$		$0.82120e-03$	
	1	$0.20490e-03$	2.00	$0.28977e-03$	1.50	$0.40980e-03$	1.00
	2	$0.68233e-04$	1.59	$0.11818e-03$	1.30	$0.20470e-03$	1.00
	3	$0.25575e-04$	1.42	$0.51150e-04$	1.21	$0.10230e-03$	1.00
	4	$0.10227e-04$	1.32	$0.22869e-04$	1.16	$0.51137e-04$	1.00
	5	$0.42609e-05$	1.26	$0.10437e-04$	1.13	$0.25565e-04$	1.00
WENO-Z	0	$0.59205e-03$		$0.59205e-03$		$0.59205e-03$	
	1	$0.14849e-03$	2.00	$0.21000e-03$	1.50	$0.29699e-03$	1.00
	2	$0.49578e-04$	1.58	$0.85872e-04$	1.29	$0.14873e-03$	1.00
	3	$0.18607e-04$	1.41	$0.37214e-04$	1.21	$0.74427e-04$	1.00
	4	$0.74458e-05$	1.32	$0.16649e-04$	1.16	$0.37229e-04$	1.00
	5	$0.31030e-05$	1.26	$0.76008e-05$	1.13	$0.18618e-04$	1.00
WENO-M	0	$0.76954e-03$		$0.76954e-03$		$0.76954e-03$	
	1	$0.19293e-03$	2.00	$0.27285e-03$	1.50	$0.38587e-03$	1.00
	2	$0.64402e-04$	1.58	$0.11155e-03$	1.29	$0.19321e-03$	1.00
	3	$0.24168e-04$	1.41	$0.48336e-04$	1.21	$0.96671e-04$	1.00
	4	$0.96706e-05$	1.32	$0.21624e-04$	1.16	$0.48353e-04$	1.00
	5	$0.40301e-05$	1.26	$0.98717e-05$	1.13	$0.24181e-04$	1.00
WENO-PZ	0	$0.12280e-04$		$0.12280e-04$		$0.12280e-04$	
	1	$0.15602e-05$	3.00	$0.22065e-05$	2.48	$0.31205e-05$	1.98
	2	$0.26219e-06$	2.57	$0.45412e-06$	2.28	$0.78656e-06$	1.99
	3	$0.49364e-07$	2.41	$0.98727e-07$	2.20	$0.19745e-06$	1.99
	4	$0.98931e-08$	2.32	$0.22122e-07$	2.16	$0.49466e-07$	2.00
	5	$0.20632e-08$	2.26	$0.50538e-08$	2.13	$0.12379e-07$	2.00
WENO-MN	0	$0.37005e-05$		$0.37005e-05$		$0.37005e-05$	
	1	$0.46276e-06$	3.00	$0.65445e-06$	2.50	$0.92553e-06$	2.00
	2	$0.77144e-07$	2.58	$0.13362e-06$	2.29	$0.23143e-06$	2.00
	3	$0.14466e-07$	2.41	$0.28932e-07$	2.21	$0.57864e-07$	2.00
	4	$0.28934e-08$	2.32	$0.64698e-08$	2.16	$0.14467e-07$	2.00
	5	$0.60280e-09$	2.26	$0.14766e-08$	2.13	$0.36168e-08$	2.00
WENO-SIF	0	$0.10396e-07$		$0.10396e-07$		$0.10396e-07$	
	1	$0.65039e-09$	4.00	$0.91979e-09$	3.50	$0.13008e-08$	3.00
	2	$0.54226e-10$	3.58	$0.93923e-10$	3.29	$0.16268e-09$	3.00
	3	$0.50850e-11$	3.41	$0.10170e-10$	3.21	$0.20340e-10$	3.00
	4	$0.50856e-12$	3.32	$0.11372e-11$	3.16	$0.25428e-11$	3.00
	5	$0.52979e-13$	3.26	$0.12977e-12$	3.13	$0.31787e-12$	3.00

Table 2 represents the various computational errors and accuracies at the $n_{cp} = 1$ critical point. The accuracy of all known WENO schemes degrades with WENO-JS and WENO-Z reduced to first-order. And the WENO-SIF scheme provided in this paper maintains the same errors and accuracies as at the zero-order critical point. That shows the WENO-NSI method can achieve optimal accuracy at the first-order critical point.

Table 3: Convergence properites of various WENO schemes at $n_{cp} = 2$ critical point.

	q	L^1-error	L^1-order	L^2-error	L^2-order	L^∞-error	L^∞-order
WENO-JS	0	$0.41613e-05$		$0.41613e-05$		$0.41613e-05$	
	1	$0.52034e-06$	3.00	$0.73587e-06$	2.50	$0.10407e-05$	2.00
	2	$0.86737e-07$	2.59	$0.15023e-06$	2.30	$0.26021e-06$	2.00
	3	$0.16265e-07$	2.42	$0.32529e-07$	2.21	$0.65058e-07$	2.00
	4	$0.32530e-08$	2.32	$0.72740e-08$	2.16	$0.16265e-07$	2.00
	5	$0.67773e-09$	2.26	$0.16601e-08$	2.13	$0.40664e-08$	2.00
WENO-Z	0	$0.38754e-05$		$0.38754e-05$		$0.38754e-05$	
	1	$0.48715e-06$	3.00	$0.68894e-06$	2.50	$0.97431e-06$	2.00
	2	$0.81420e-07$	2.58	$0.14102e-06$	2.29	$0.24426e-06$	2.00
	3	$0.15288e-07$	2.41	$0.30576e-07$	2.21	$0.61151e-07$	2.00
	4	$0.30597e-08$	2.32	$0.68417e-08$	2.16	$0.15299e-07$	2.00
	5	$0.63766e-09$	2.26	$0.15619e-08$	2.13	$0.38260e-08$	2.00
WENO-M	0	$0.41505e-05$		$0.41505e-05$		$0.41505e-05$	
	1	$0.51918e-06$	3.00	$0.73424e-06$	2.50	$0.10384e-05$	2.00
	2	$0.86560e-07$	2.58	$0.14993e-06$	2.29	$0.25968e-06$	2.00
	3	$0.16233e-07$	2.41	$0.32466e-07$	2.21	$0.64931e-07$	2.00
	4	$0.32468e-08$	2.32	$0.72601e-08$	2.16	$0.16234e-07$	2.00
	5	$0.67645e-09$	2.26	$0.16570e-08$	2.13	$0.40587e-08$	2.00
WENO-PZ	0	$0.26182e-07$		$0.26182e-07$		$0.26182e-07$	
	1	$0.13981e-08$	4.23	$0.19772e-08$	3.73	$0.27962e-08$	3.23
	2	$0.99909e-10$	3.81	$0.17305e-09$	3.51	$0.29973e-09$	3.22
	3	$0.81698e-11$	3.61	$0.16340e-10$	3.40	$0.32679e-10$	3.20
	4	$0.72873e-12$	3.49	$0.16295e-11$	3.33	$0.36437e-11$	3.16
	5	$0.69272e-13$	3.40	$0.16968e-12$	3.26	$0.41563e-12$	3.13
WENO-MN	0	$0.40817e-05$		$0.40817e-05$		$0.40817e-05$	
	1	$0.51074e-06$	3.00	$0.72229e-06$	2.50	$0.10215e-05$	2.00
	2	$0.85165e-07$	2.58	$0.14751e-06$	2.29	$0.25550e-06$	2.00
	3	$0.15973e-07$	2.41	$0.31945e-07$	2.21	$0.63890e-07$	2.00
	4	$0.31949e-08$	2.32	$0.71440e-08$	2.16	$0.15974e-07$	2.00
	5	$0.66565e-09$	2.26	$0.16305e-08$	2.13	$0.39939e-08$	2.00
WENO-SIF	0	$0.10396e-07$		$0.10396e-07$		$0.10396e-07$	
	1	$0.65039e-09$	4.00	$0.91979e-09$	3.50	$0.13008e-08$	3.00
	2	$0.54226e-10$	3.58	$0.93923e-10$	3.29	$0.16268e-09$	3.00
	3	$0.50850e-11$	3.41	$0.10170e-10$	3.21	$0.20340e-10$	3.00
	4	$0.50856e-12$	3.32	$0.11372e-11$	3.16	$0.25428e-11$	3.00
	5	$0.52979e-13$	3.26	$0.12977e-12$	3.13	$0.31787e-12$	3.00

Table 3 represents the various computational errors and accuracies for $n_{cp} = 2$. The results show that the accuracy of the methods WENO-JS, WENO-Z, and WENO-M decreases to the second-order at the second-order critical point, and the WENO-PZ can achieve the third-order accuracy. In contrast, the WENO-SIF scheme has the smallest various errors and maintains the theoretical third-order accuracy.

4.2. One-dimensional Linear advection problems

The main work of this subsection is to examine the resolution and computational efficiency of various WENO schemes in computing the following 1D advection equation

$$\begin{cases} u_t + u_x = 0, \quad x \in [a,\ b], \\ u(x,0) = u_0(x),\ \text{periodic boundary.} \end{cases} \tag{34}$$

4.2.1. Case 1:

The initial conditions of this case are

$$u_0(x) = \begin{cases} 1,\ x \in [-1,0), \\ 0,\ x \in [0,1]. \end{cases} \tag{35}$$

Figure 4 represents the numerical solutions of various WENO methods using 200 consistent cells with $t = 2$. We can see that the results of WENO-SIF are closer to the exact, while WENO-PZ shows nonphysical oscillations. That shows the present WENO-SIF is numerically stable and far less dissipative than the other WENO schemes.

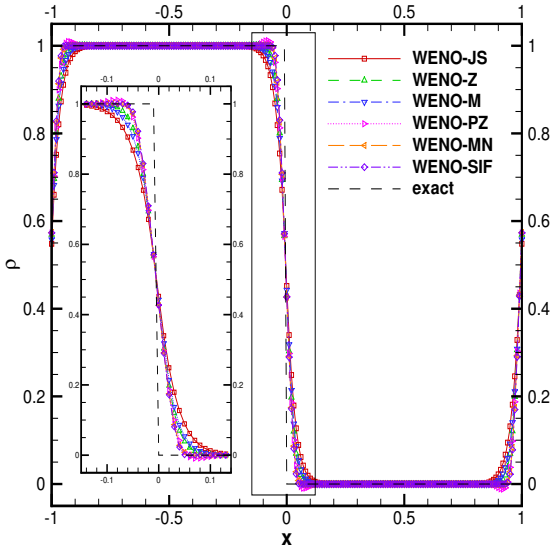

Fig. 4: Results of linear advection equation case 1 for various WENO methods with 200 cells.

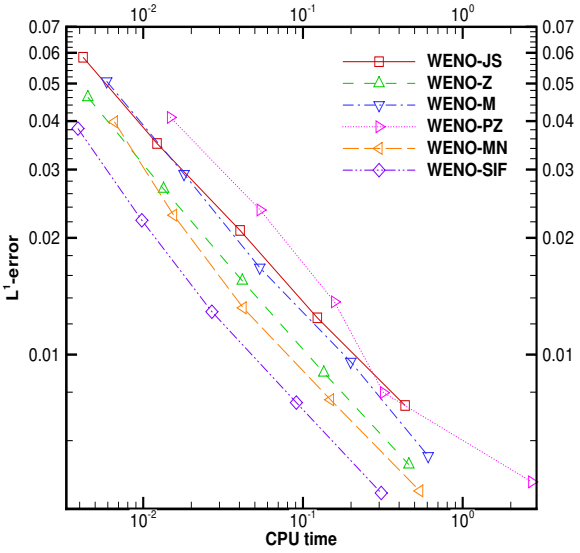

Fig. 5: Computational efficiency for linear advection equation case 1.

Table 4: Comparison of L^1-errors and CPU times of various methods for Case 1 at $t = 2$.

	N	100	200	400	800	1600
WENO-JS	L^1-error	$0.58435e-01$	$0.35024e-01$	$0.20901e-01$	$0.12440e-01$	$0.73929e-02$
	Time(s)	0.0042	0.0122	0.0404	0.1230	0.4359
WENO-Z	L^1-error	$0.46070e-01$	$0.26750e-01$	$0.15503e-01$	$0.89808e-02$	$0.52044e-02$
	Time(s)	0.0045	0.0134	0.0417	0.1350	0.4602
WENO-M	L^1-error	$0.50682e-01$	$0.29236e-01$	$0.16767e-01$	$0.95875e-02$	$0.54771e-02$
	Time(s)	0.0059	0.0180	0.0536	0.1989	0.6077
WENO-PZ	L^1-error	$0.40887e-01$	$0.23599e-01$	$0.13677e-01$	$0.79797e-02$	$0.46984e-02$
	Time(s)	0.0148	0.0539	0.1575	0.3191	2.7030
WENO-MN	L^1-error	$0.39833e-01$	$0.22884e-01$	$0.13199e-01$	$0.76482e-02$	$0.44515e-02$
	Time(s)	0.0066	0.0155	0.0422	0.1488	0.5384
WENO-SIF	L^1-error	$0.38276e-01$	$0.22199e-01$	$0.12898e-01$	$0.75204e-02$	$0.43977e-02$
	Time(s)	0.0039	0.0098	0.0269	0.0909	0.3089

In this example, we also compare the L^1 errors and CPU times of various schemes in computing this problem using different grid numbers, and the results are shown in Tab. 4 and Fig.5. The results show the CPU times of WENO-SIF are significantly less than these WENO schemes when computing this problem. And all the errors of WENO-SIF are significantly smaller than those of the other schemes. That shows the WENO-SIF scheme has far better resolution and higher efficiency than others.

4.2.2. Case 2:

The initial conditions of this case are

$$u_0(x) = \begin{cases} \frac{1}{6}(G(x,\beta,z-\delta)+G(x,\beta,z+\delta)+4G(x,\beta,z)), & x\in[-0.8,-0.6), \\ 1, & x\in[-0.4,-0.2), \\ 1-|10(x-0.1)|, & x\in[0,0.2), \\ \frac{1}{6}(F(x,\alpha,a-\delta)+F(x,\alpha,a+\delta)+4F(x,\alpha,z)), & x\in[0.4,0.6), \\ 0, & otherwise, \end{cases} \tag{36}$$

where $G(x,\beta,z) = e^{-\beta(x-z)^2}$, $F(x,\alpha,a) = \sqrt{max(1-\alpha^2(x-a)^2,0)}$ and the constants $z=-0.7$, $\delta = 0.0005$, $\beta = ln2/(36\delta^2)$ and $\alpha = 10$. Figure 6 represents the numerical solutions of various WENO methods using 200 consistent cells with $t = 6$. In the square wave region (A), the results of both WENO-PZ and WENO-MN schemes show an upward jump, while the three schemes WENO-JS, WENO-Z, and WENO-M do not capture the square wave. In contrast, the present WENO-SIF is able to recognize the square wave and has a better match with the exact solution. And at the junction of square and triangular waves (B), the WENO-SIF provided in this paper performs significantly better than other WENO schemes. That shows the WENO-SIF scheme has better resolution than the others.

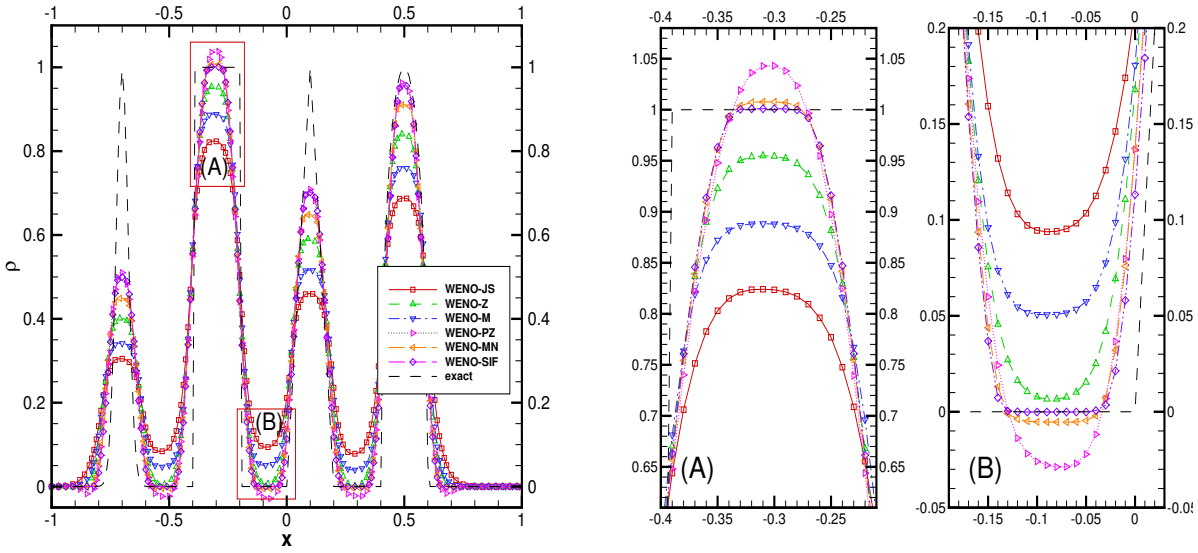

Fig. 6: Results of Case 2 for various WENO methods with 200 cells at $t = 6$.

Table 5: Comparison of L^1-errors and CPU times of various methods for Case 1 at $t = 2$ s.

	N	100	200	400	800	1600
WENO-JS	L^1-error	$0.26205e+00$	$0.15034e+00$	$0.70698e-01$	$0.35678e-01$	$0.16544e-01$
	Time(s)	0.0143	0.0402	0.1161	0.3631	1.2816
WENO-Z	L^1-error	$0.21769e+00$	$0.96672e-01$	$0.43808e-01$	$0.20840e-01$	$0.96340e-02$
	Time(s)	0.0148	0.0134	0.1203	0.3935	1.3887
WENO-M	L^1-error	$0.24688e+00$	$0.11729e+00$	$0.49859e-01$	$0.23715e-01$	$0.10502e-01$
	Time(s)	0.0186	0.0530	0.1658	0.1989	1.8517
WENO-PZ	L^1-error	$0.15722e+00$	$0.70561e-01$	$0.33124e-01$	$0.15816e-01$	$0.79290e-02$
	Time(s)	0.0405	0.1495	0.4392	0.9634	8.1953
WENO-MN	L^1-error	$0.18516e+00$	$0.75132e-01$	$0.34745e-01$	$0.16311e-01$	$0.76641e-02$
	Time(s)	0.0173	0.0448	0.1358	0.4517	1.6231
WENO-SIF	L^1-error	$0.14108e+00$	$0.64001e-01$	$0.31129e-01$	$0.14958e-01$	$0.73013e-02$
	Time(s)	0.0133	0.0352	0.0933	0.2795	0.9567

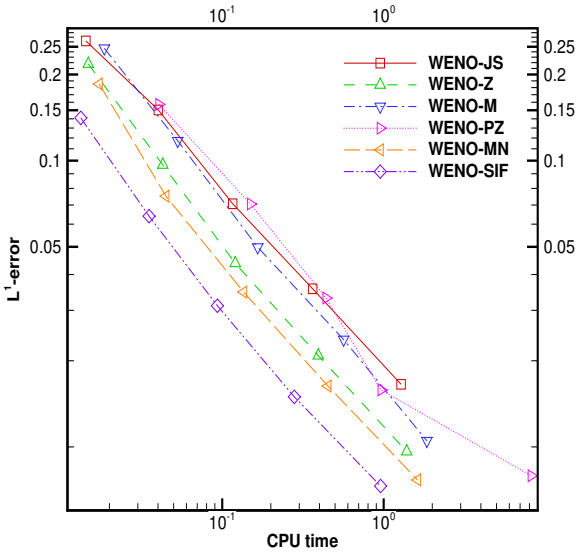

Fig. 7: Computational efficiency for linear advection equation case 2.

We also compare the L^1 error and CPU time when computing this problem using different WENO schemes, and the results are presented in Tab. 5 and Fig. 7. That shows the CPU times of WENO-SIF are significantly less than the other WENO schemes, and the errors are also less than the other schemes. That shows the WENO-SIF scheme has good resolution and high efficiency than others.

4.3. One-dimensional inviscid Burgers equation

Next, we will solve the one-dimensional linear inviscid Burgers equation of the following form

$$\begin{cases} u_t + uu_x = 0, \quad x \in [0,\ 2\pi], \\ u_0(x) = 0.5 + 0.5sin(x),\ \text{periodic boundary}. \end{cases} \tag{37}$$

Figure 8 represents the numerical solutions of Burgers equation using 100 consistent cells with $t = 3$, where the reference solution is the result of third-order WENO-JS with 8000 cells. See from the enlarged view at the discontinuity point, the results of WENO-SIF are closer to the exact solution than the other schemes.

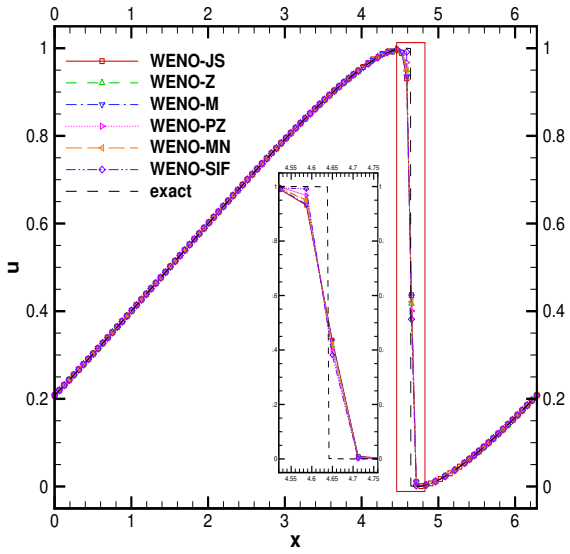

Fig. 8: Results of inviscid Burgers's problem for various WENO methods with 100 cells.

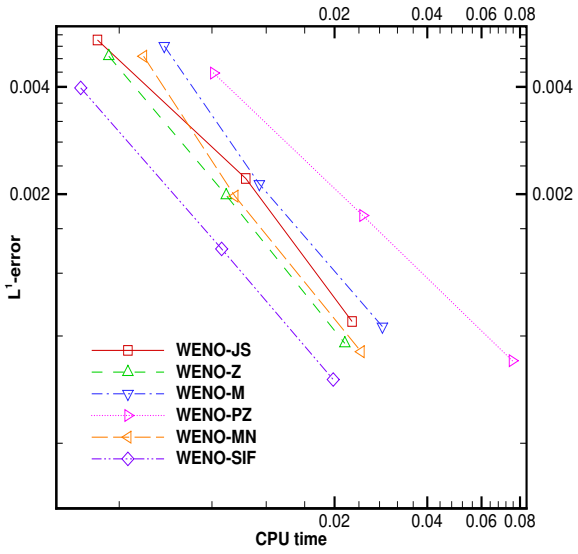

Fig. 9: Computational efficiency for inviscid Burgers's problem.

We also compare the L^1 error and CPU time for this problem, and the results are presented in Tab. 6 and Fig. 9. The results show that WENO-SIF requires significantly less CPU time than other WENO schemes to compute this problem with higher accuracy. That shows the WENO-SIF scheme has a higher resolution and computational efficiency than other WENO schemes.

Table 6: Comparison of L^1-errors and CPU times of various methods for Burgers equation at $t = 3$.

	N	100	200	400
WENO-JS	L^1-error	$0.54154e-02$	$0.22134e-02$	$0.87846e-03$
	Time(s)	0.0034	0.0103	0.0228
WENO-Z	L^1-error	$0.48777e-02$	$0.19846e-02$	$0.76258e-03$
	Time(s)	0.0037	0.0089	0.0216
WENO-M	L^1-error	$0.52125e-02$	$0.21352e-02$	$0.85026e-03$
	Time(s)	0.0056	0.0114	0.0286
WENO-PZ	L^1-error	$0.43732e-02$	$0.17424e-02$	$0.68191e-03$
	Time(s)	0.0081	0.0247	0.0755
WENO-MN	L^1-error	$0.48761e-02$	$0.19743e-02$	$0.72258e-03$
	Time(s)	0.0048	0.0095	0.0244
WENO-SIF	L^1-error	$0.39736e-02$	$0.14041e-02$	$0.60373e-03$
	Time(s)	0.0030	0.0086	0.0198

4.4. One-dimensional gas dynamic Euler equations

This section focuses on performing various WENO schemes for the 1-D gas dynamic Euler equation.

$$\mathbf{u}_t + f(\mathbf{u})_x = 0, \tag{38}$$

with

$$\mathbf{u} = (\rho, \rho u, E)^T, \quad f(\mathbf{u}) = (\rho u, \rho u^2 + p, u(E+p))^T, \tag{39}$$

where $\rho,\ u,\ p$ are the density, velocity and pressure, respectively. $E = p/(\gamma - 1) + \frac{1}{2}\rho u^2$ is the total energy and γ is the specific heat ratio is set as $\gamma = 1.4$. And the time step is

$$\Delta t = \frac{CFL\Delta x}{max_i(u_i + c_i)} \tag{40}$$

where $c = \sqrt{\gamma p/\rho}$. We will use the global Lax-Friedrichs flux splitting method in each of the following examples, and the numerical fluxes are reconstructed in the characteristic space.

4.4.1. SOD's problem

The initial conditions of SOD's problem are

$$(\rho, u, p) = \begin{cases} (0.125, 0, 0.1), & x \in [0, 0.5], \\ (1.000, 0, 1.0), & x \in (0.5, 1]. \end{cases} \tag{41}$$

Fig. 10 represents the density profiles of various WENO schemes at 200 cells until $t = 0.2$ with the reference solution calculated with WENO-JS at 4000 cells. Results in the local zoom-in plots show that the results of WENO-SIF are closer to the reference solution than the other WENO schemes.

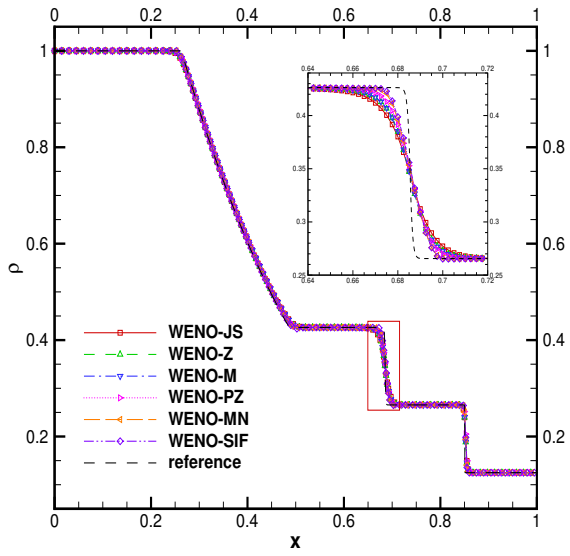

Fig. 10: Results of SOD's problem for various WENO methods with 400 cells.

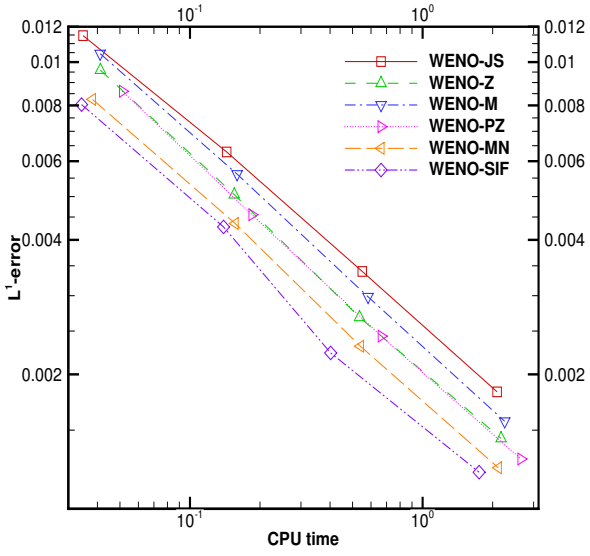

Fig. 11: Computational efficiency for SOD's problem.

In this example, we also compare the L^1 errors and CPU times of various schemes in computing this problem using different grid numbers, and the results are shown in Tab. 7 and Fig.11. It is easy to see that the WENO-SIF scheme has the least CPU time, and its error is the smallest among the results of all WENO schemes. That shows the present WENO-SIF has optimal computational efficiency.

Table 7: Comparison of L^1-errors and CPU times of various methods for SOD's problem at $t = 0.2$.

	N	100	200	400	800
WENO-JS	L^1-error	$0.11463e-01$	$0.62931e-02$	$0.33992e-02$	$0.18274e-02$
	Time(s)	0.0347	0.1438	0.5502	2.0903
WENO-Z	L^1-error	$0.95978e-02$	$0.50504e-02$	$0.26840e-02$	$0.14375e-02$
	Time(s)	0.0412	0.1550	0.5355	2.1739
WENO-M	L^1-error	$0.10447e-01$	$0.56146e-02$	$0.29825e-02$	$0.15702e-02$
	Time(s)	0.0411	0.1594	0.5828	2.2522
WENO-PZ	L^1-error	$0.86036e-02$	$0.45538e-02$	$0.24355e-02$	$0.12930e-02$
	Time(s)	0.0513	0.1847	0.6636	2.6458
WENO-MN	L^1-error	$0.82540e-02$	$0.43519e-02$	$0.23119e-02$	$0.12356e-02$
	Time(s)	0.0381	0.1564	0.5404	2.1155
WENO-SIF	L^1-error	$0.80335e-02$	$0.42763e-02$	$0.22335e-02$	$0.12078e-02$
	Time(s)	0.0342	0.1394	0.4027	1.7492

4.4.2. Shu-Osher's problem

The initial conditions of Shu-Osher's problem at $[-5, 5]$ are as follows

$$(\rho, u, p) = \begin{cases} (3.857143, 2.629369, 10.33333), & x \in [-5, -4), \\ (1 + 0.2sin(5\pi x), 0, 1), & otherwise. \end{cases} \tag{42}$$

This problem contains low-frequency and high-frequency density disturbances and is used to test the performance of different WENO methods. Fig.12 presents the distribution curves of density for various WENO methods with 400 cells at $t = 1.8$. The reference solution is calculated by using WENO-JS with 4000 cells. See from the figure, WENO-SIF performs better than other WENO methods.

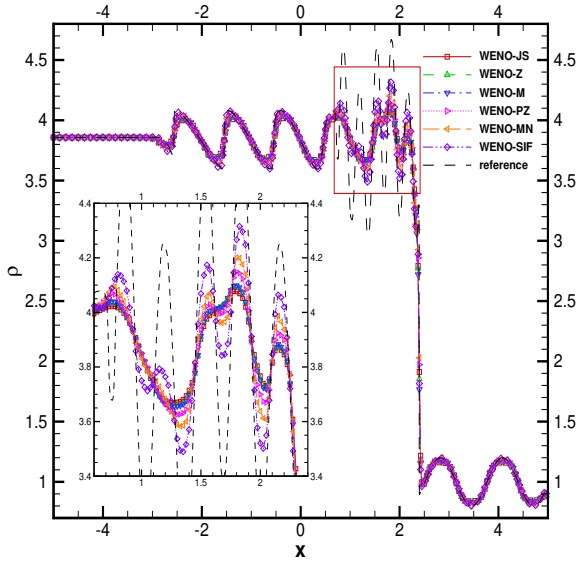

Fig. 12: Results of Shu-Osher's problem for various WENO methods with 400 cells.

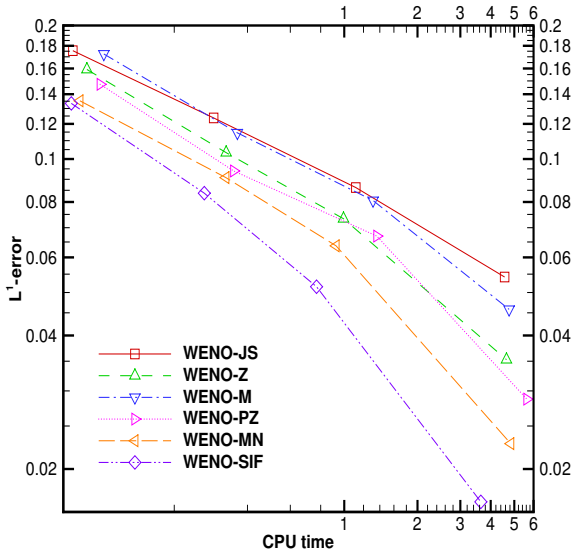

Fig. 13: Computational efficiency for Shu-Osher's problem.

The L^1 errors and CPU times for this case with selected grid numbers are shown in Tab. 8 and Fig.13. It is easy to see that the WENO-SIF scheme has the least CPU time, and its error is the smallest among the results of all WENO schemes. That shows the present WENO-SIF has optimal computational efficiency.

Table 8: Comparison of L^1-errors and CPU times of various methods for Shu-Osher's problem at $t = 1.8$.

	N	100	200	400	800
WENO-JS	L^1-error	$0.17548e+00$	$0.12377e+00$	$0.86223e-01$	$0.54189e-01$
	Time(s)	0.0766	0.2905	1.1156	4.5627
WENO-Z	L^1-error	$0.15919e+00$	$0.10336e+00$	$0.73338e-01$	$0.35291e-01$
	Time(s)	0.0875	0.3269	0.9927	4.6423
WENO-M	L^1-error	$0.17251e+00$	$0.11455e+00$	$0.80621e-01$	$0.45814e-01$
	Time(s)	0.1027	0.3636	1.3128	4.7600
WENO-PZ	L^1-error	$0.14736e+00$	$0.93986e-01$	$0.67015e-01$	$0.28745e-01$
	Time(s)	0.0992	0.3511	1.3608	5.6314
WENO-MN	L^1-error	$0.13527e+00$	$0.90792e-01$	$0.63716e-01$	$0.22812e-01$
	Time(s)	0.0819	0.3261	0.9253	4.8361
WENO-SIF	L^1-error	$0.13348e+00$	$0.83750e-01$	$0.51532e-01$	$0.16863e-01$
	Time(s)	0.0755	0.2658	0.7691	3.6428

4.4.3. Titarev-Toro's problem

The initial conditions of the problem as follows

$$(\rho, u, p) = \begin{cases} (1.515695, 0.523346, 1.805000), & x \in [-5, -4.5), \\ (1 + 0.1sin(20\pi x), 0, 1), & x \in [-4.5, 5]. \end{cases} \tag{43}$$

Figure 14 represents the computational results of various WENO methods using 2000 cells at $t = 5$. The reference solution is computed by using third-order WENO-JS at 8000 cells. See from the figure that WENO-SIF performs better than the other WENO schemes.

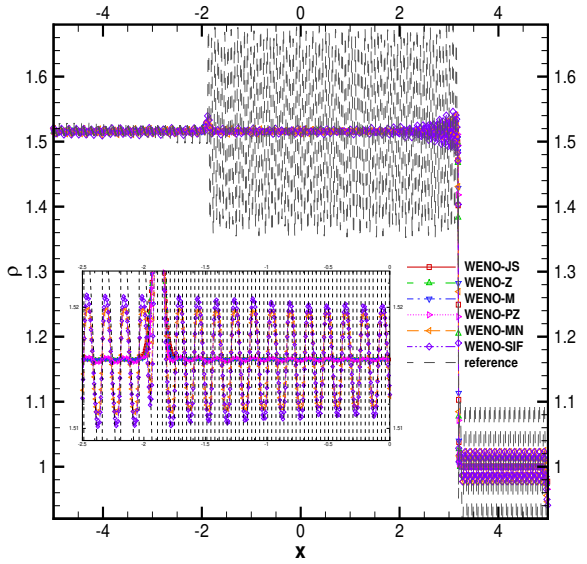

Fig. 14: Results of Titarev-Toro's problem for various WENO methods with 2000 cells.

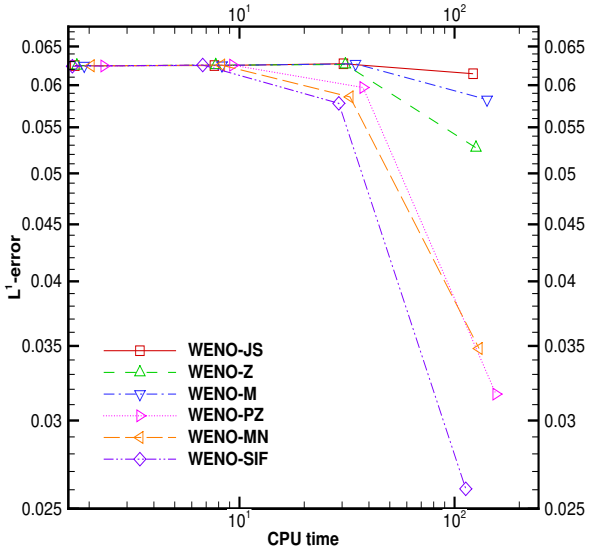

Fig. 15: Computational efficiency for Titarev-Toro's problem.

The L^1 errors and CPU times for the problem on the selected grid are shown in Tab. 9 and Fig. 15. It is easy to see that the WENO-SIF scheme takes much less CPU time to compute the problem and its accuracy is higher than that of the others. That indicates the present WENO-SIF has the best resolution and computational efficiency.

Table 9: Comparison of L^1-errors and CPU times of various methods for Titarev-Toro's problem at $t = 5$.

	N	500	1000	2000	4000
WENO-JS	L^1-error	$0.62483e-01$	$0.62483e-01$	$0.62718e-01$	$0.61440e-01$
	Time(s)	1.7156	7.6427	30.439	121.97
WENO-Z	L^1-error	$0.62460e-01$	$0.62530e-01$	$0.62618e-01$	$0.52714e-01$
	Time(s)	1.7536	7.7542	31.077	125.80
WENO-M	L^1-error	$0.62464e-01$	$0.62506e-01$	$0.62707e-01$	$0.58239e-01$
	Time(s)	1.8969	8.2901	34.635	141.58
WENO-PZ	L^1-error	$0.62428e-01$	$0.62532e-01$	$0.59712e-01$	$0.31684e-01$
	Time(s)	2.3443	9.3078	37.529	155.85
WENO-MN	L^1-error	$0.62453e-01$	$0.62538e-01$	$0.58557e-01$	$0.34812e-01$
	Time(s)	2.0427	8.2568	32.641	130.05
WENO-SIF	L^1-error	$0.62396e-01$	$0.62550e-01$	$0.57788e-01$	$0.26048e-01$
	Time(s)	1.6708	6.7469	28.965	112.78

4.5. Two dimension gas dynamic Euler equation

In this section, we will investigate the performance characteristics of the WENO scheme mentioned in this paper by solving a two-dimensional gas dynamics problem of the following form

$$\mathbf{u}_t + f(\mathbf{u})_x + g(\mathbf{u})_y = 0, \tag{44}$$

with

$$\begin{aligned} \mathbf{u} &= (\rho, \rho u, \rho v, E)^T, \\ f(\mathbf{u}) &= (\rho u, \rho u^2 + p, \rho uv, u(E+p))^T, \\ g(\mathbf{u}) &= (\rho v, \rho uv, \rho v^2 + p, v(E+p))^T, \end{aligned} \tag{45}$$

where, $\rho,\ u,\ v,\ p$ are the density, x-velocity, y-velocity and pressure, respectively. And the total energy E is defined as

$$E = \frac{p}{\gamma - 1} + \frac{1}{2}\rho(u^2 + v^2) \tag{46}$$

And the time step is

$$\Delta t = \frac{CFL\Delta x \Delta y}{max_i(u_i + c_i) + max_j(v_j + c_j)} \tag{47}$$

where $c = \sqrt{\gamma p/\rho}$ and $CFL = 0.6$. We will use the global Lax-Friedrichs flux splitting method in each of the following examples, and the numerical fluxes are reconstructed in the characteristic space. The specific heat ratio $\gamma = 1.4$ for all examples except $\gamma = 5/3$ in RT instability problem.

4.5.1. 2-D Riemann Problem: case 1

The initial conditions for 2-dimensional Riemann problem are as following[46, 48, 51]

$$(\rho, u, v, p) = \begin{cases} (1.5, 0.0, 0.0, 1.5), & 0.8 \le x \le 1,\ 0.8 \le y \le 1, \\ (0.5323, 1.2, 0, 0.3), & 0 \le x < 0.8,\ 0.8 \le y \le 1, \\ (0.138, 1.206, 1.206, 0.029), & 0 \le x < 0.8,\ 0 \le y < 0.8, \\ (0.5323, 0.0, 1.206, 0.3), & 0.8 < x \le 1,\ 0 \le y < 0.8. \end{cases} \tag{48}$$

In the results, there is a mushroom-like structure symmetric about the diagonal $y = x$, and the richness of the vortex structure at the interface can usually examine the resolution of the different schemes. The boundary conditions for this problem are: all four edges are zero-order extrapolation. Figure 16 represents the density contours of this case by using 800×800 cells until $t = 0.8$ with 24 contours at [0.2,1.7]. One can see that the unstable Kelvin-Helmholtz microstructures constructed by WENO-SIF are significantly more abundant than the other WENO schemes, showing that the present scheme has better resolution than the rest.

4.5.2. 2-D Riemann Problem: case 2

The initial conditions for 2-dimensional Riemann problem are as following[46, 48, 51]

$$(\rho, u, v, p) = \begin{cases} (3, -0.75, -0.5, 1), & 0.5 \le x \le 1,\ 0.5 \le y \le 1, \\ (2, 0.75, 0.5, 1), & 0 \le x < 0.5,\ 0.5 \le y \le 1, \\ (1, -0.75, 0.5, 1), & 0 \le x < 0.5,\ 0 \le y < 0.5, \\ (1, 0.75, -0.5, 1), & 0.5 < x \le 1,\ 0 \le y < 0.5. \end{cases} \tag{49}$$

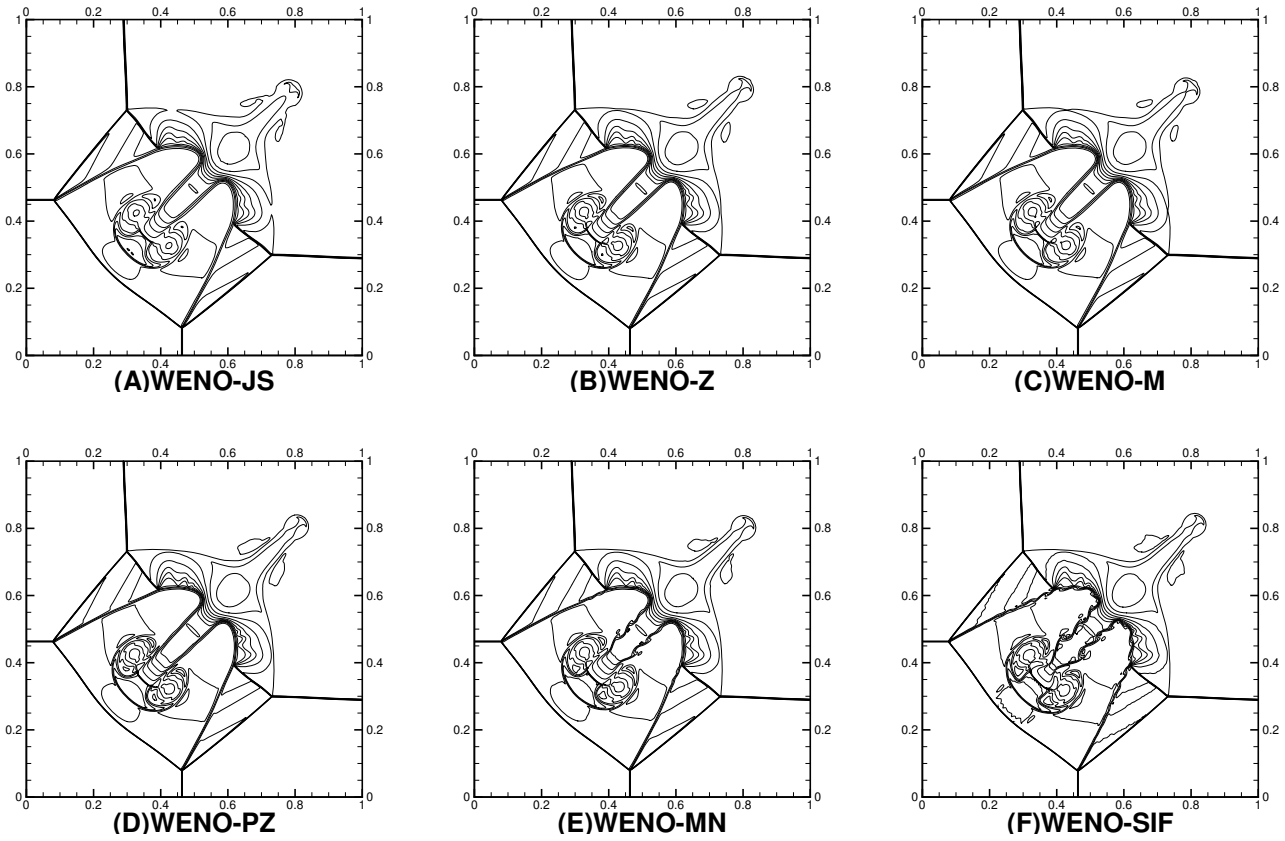

Fig. 16: Results of 2-D Riemann Problem for case 1: 20 density contours at $[0.2,\ 2.2]$ with 640×640 cells.

All four edges of the problem are zero-order extrapolation boundary conditions. Figure 17 shows the density contours for the various WENO schemes using 800×800 cells until $t = 0.8$ with 20 contours at [0.2,2.2]. Comparing the computational results of the various schemes shows that the unstable Kelvin-Helmholtz microstructure constructed by WENO-SIF is significantly more abundant than other WENO schemes.

4.5.3. Implosion Problem

This problem is usually used to test the ability of numerical schemes to capture contact discontinuities and maintain symmetry: if the scheme does not maintain symmetry, the jet will be distorted[49, 50]. The initial conditions

$$(\rho, u, v, p) = \begin{cases} (0.125, 0, 0, 0.14), & 0 \leq |x| + |y| < 0.15, \\ (1, 0, 0, 1), & \text{otherwise.} \end{cases} \tag{50}$$

All four edges of the problem are reflection boundaries. Figure 18 shows the density contours for the various WENO schemes using 800×800 cells until $t = 2.5$ with 12 contours at [0.45,1.0]. Comparing the jets on the diagonal in each graph, we can see that the length of WENO-SIF (F) is longer than others. That shows the present scheme is better than the rest in computing this problem.

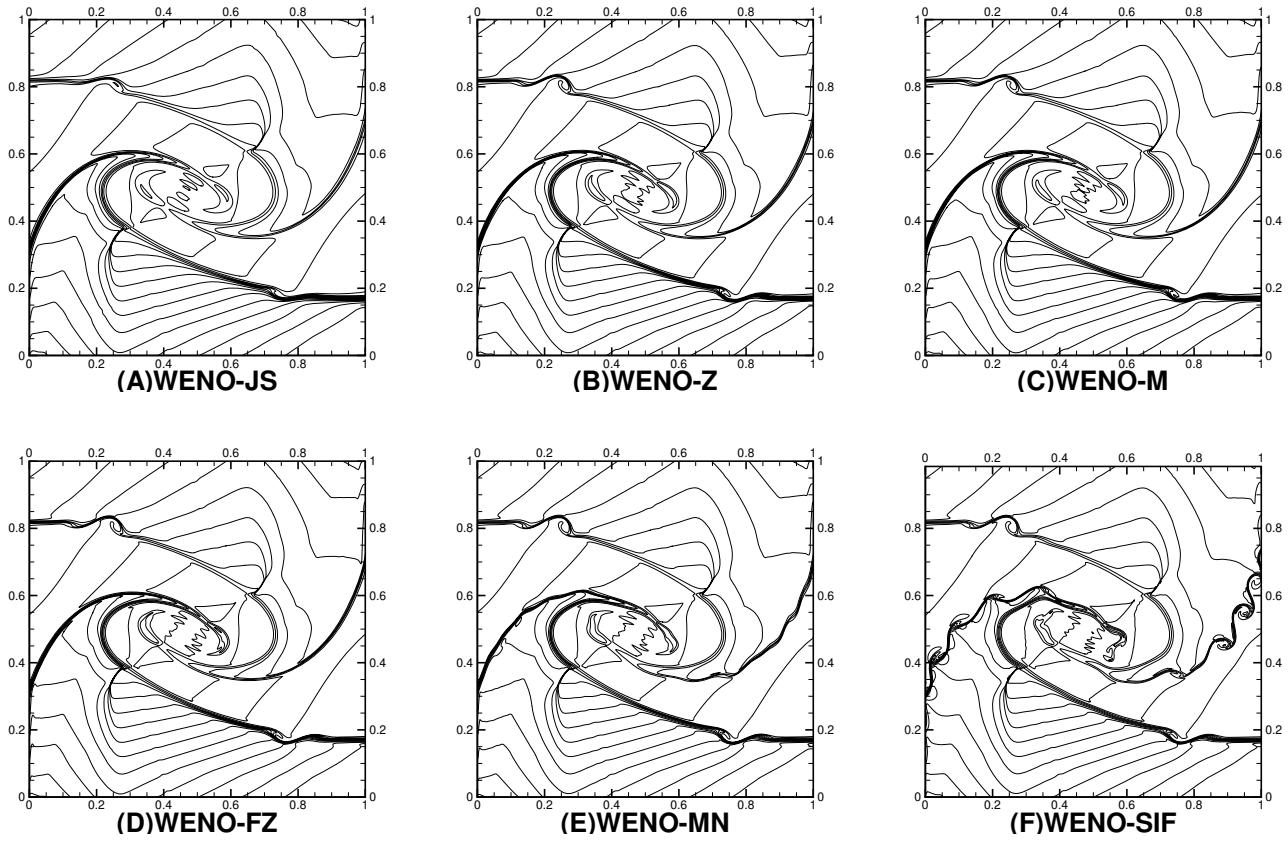

Fig. 17: Results of 2-D Riemann Problem for case 2: 20 density contours at $[0.2,\ 2.2]$ with 800×800 cells.

4.5.4. Double-Mach reflection problem

This problem has widely used as a test example for high-order schemes. The initial conditions of double-Mach reflection problem on the computational region $[0, 4] \times [0, 1]$ given as[3, 13, 47]

$$(\rho,\ u,\ v,\ p) = \begin{cases} (8, 57.1597, -33.0012, 563.544), & y < \sqrt{3}(x - 1/6), \\ (1.4, 0, 0, 2.5), & y \geq \sqrt{3}(x - 1/6), \end{cases} \tag{51}$$

The boundary conditions for this problem are: on the bottom, exact post-shock conditions are imposed in the interval $[0, 1/6]$, and we use the reflection boundary for the rest. We set the top to be the exact motion of a Mach 10 shock. Inflow and outflow for the left and right, respectively. Figure 19 shows the density contours for the various WENO schemes using 1024×256 cells until $t = 0.2$ with 30 contours at [2,22]. At the interface, WENO-SIF has a richer vortex structure than the rest of the solutions. That shows the present WENO-SIF has a better resolution than others.

4.5.5. RT instability problem

The initial conditions on the computational region $[0, 0.25] \times [0, 1]$ given as[12, 49, 50]

$$(\rho, u, v, p) = \begin{cases} (2, 0, -0.025\sqrt{\gamma p/\rho} cos(8\pi x), 2y + 1), & 0 \leq y < 0.5, \\ (1, 0, -0.025\sqrt{\gamma p/\rho} cos(8\pi x), y + 1.5), & 0.5 \leq y < 1. \end{cases} \tag{52}$$

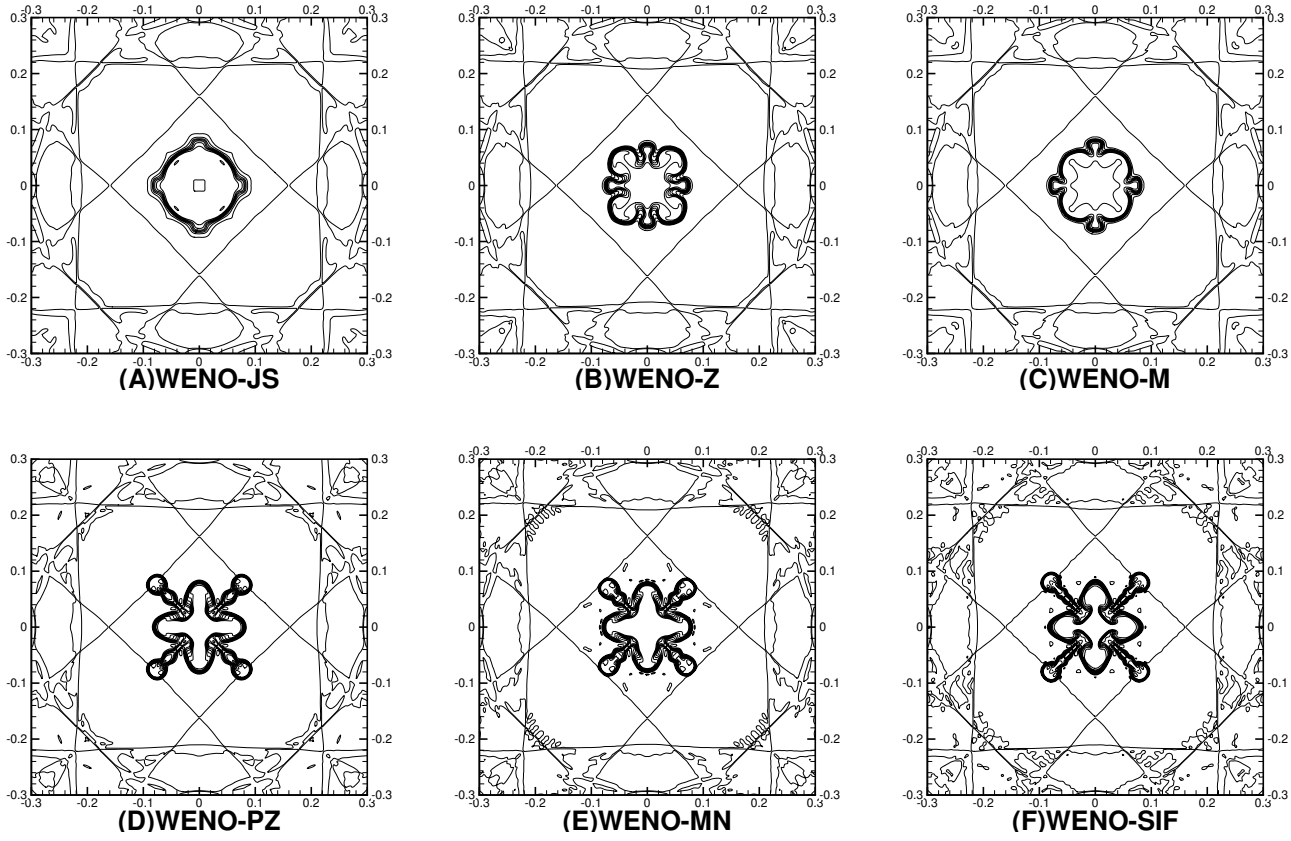

Fig. 18: Results of Implosion Problem: 12 density contours at $[0.45,\ 1.0]$ with 800×800 cells.

This problem, as a benchmark, examines the performance of various schemes to capture complex vortex structures and maintain symmetry. We set the boundaries of the problem: the bottom and top are the incoming and outgoing flow boundaries, respectively, and both the left and right are the reflection boundaries. Figure 20 shows the density contour profiles for various WENO methods using 256×1024 grids up to $t = 1.95$, 13 density contours at $[0.9,\ 2.2]$. Comparing the results of all schemes, one can see that the present WENO-SIF has the richest vortex structure and keeps symmetry.

4.5.6. Forward-facing step problem

The problem describes a supersonic fluid of Mach 3 entering a tunnel with a step reflected several times on the surface, thus generating a shock wave of the disembodied body. This problem is commonly used to test the numerical stability and resolution of different numerical schemes. The wind tunnel has a length of 3, a width of 1, and a step of 0.2 in height is at 0.6 of the wind tunnel. $(\rho, u, v, p) = (1.0, 3.0, 0, 0, 0.71429)$ is on the left side of the wind tunnel, and outflow boundary conditions on the right side. The surfaces of both the tunnel and the step are reflection boundaries. Figure 21 shows the density contour profiles for various WENO methods using 900×300 grids at $t = 4.0$, 45 density contours at $[0.5,\ 6.0]$. At the interface of these shocks, WENO-SIF has a richer vortex structure than others. That indicates the present WENO-SIF has a better resolution than other WENO schemes.

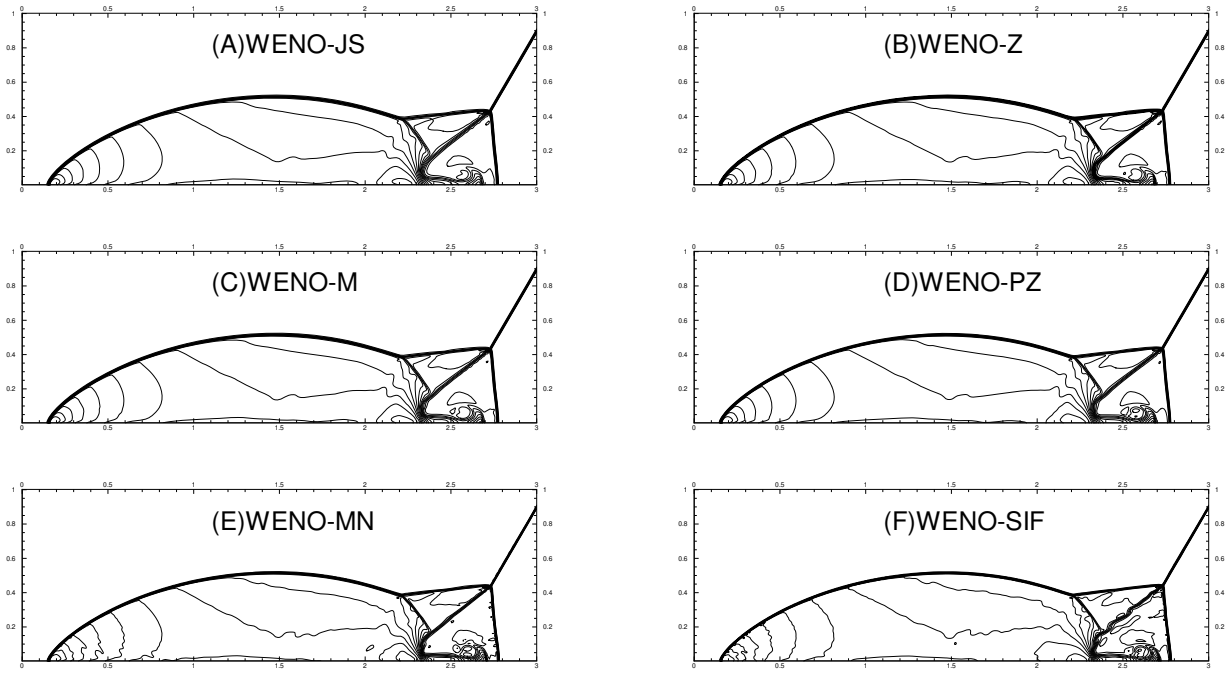

Fig. 19: Results of Implosion Problem: 30 density contours at $[2,\ 22]$ with 1024×256 cells.

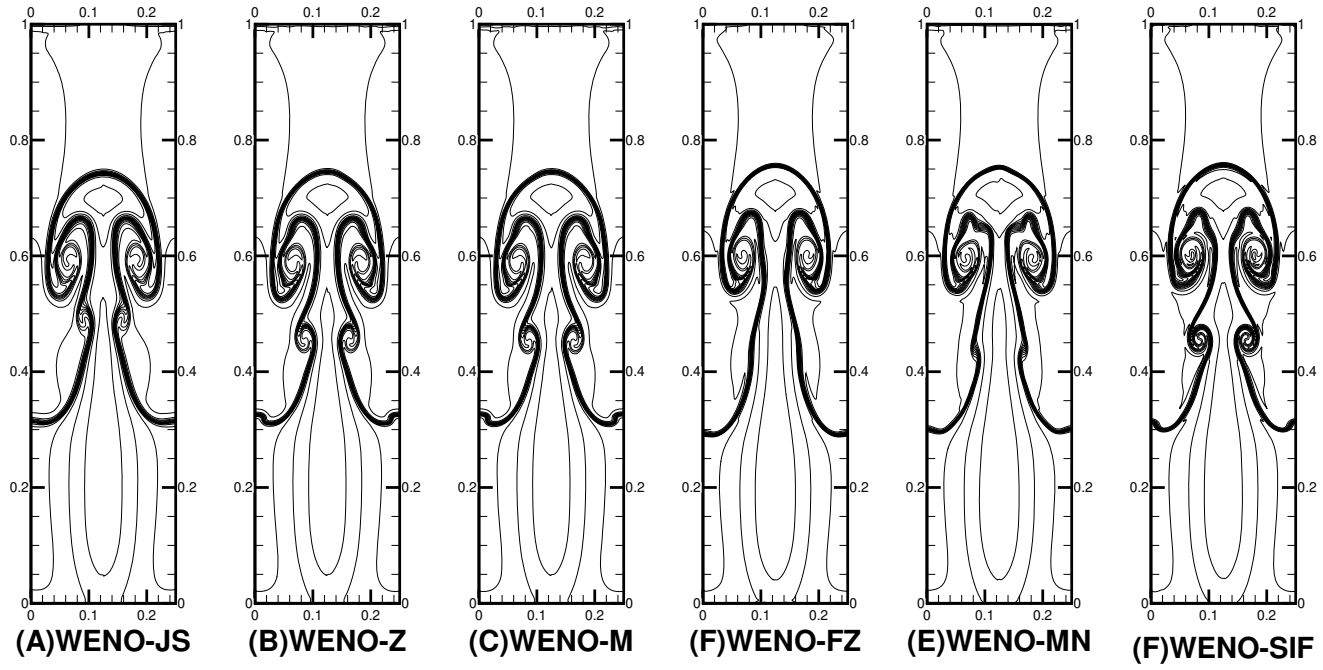

Fig. 20: Results of RT instability Problem: 13 density contours at $[0.9,\ 2.2]$ with 256×1024 cells.

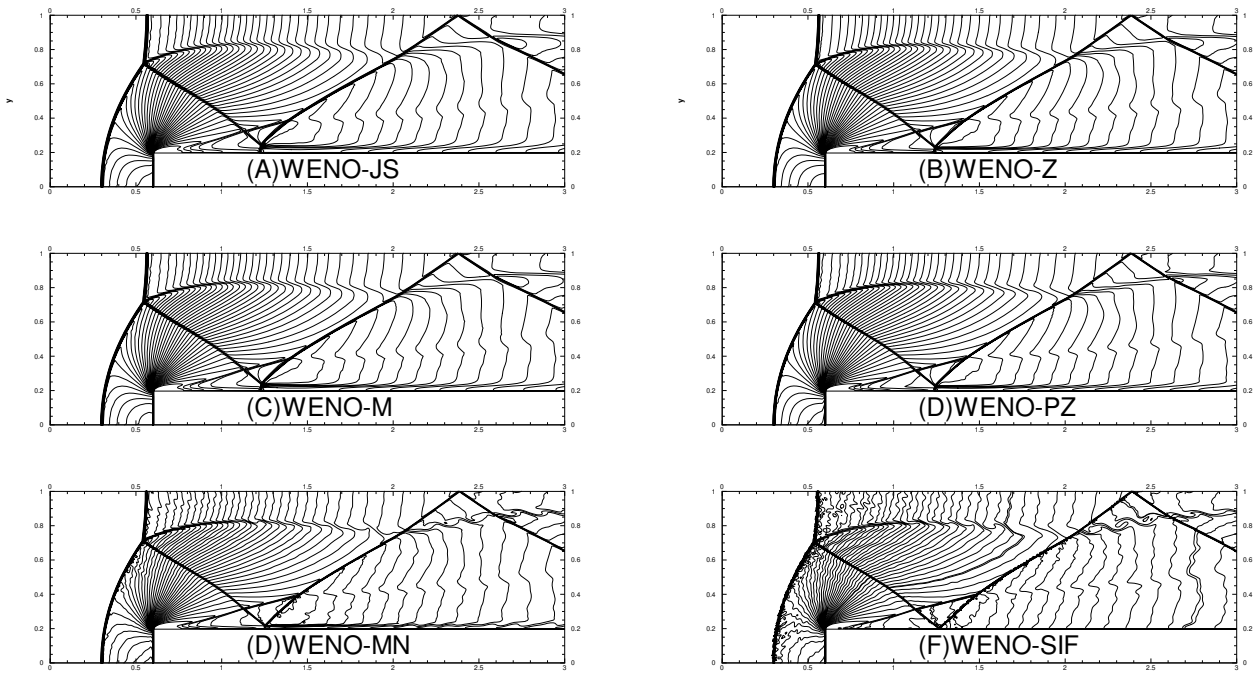

Fig. 21: Results of Forward-facing step problem: 45 density contours at $[0.5,\ 6.0]$ with 900×300 cells.

4.5.7. Kelvin-Helmholtz instability problem

The initial conditions on the computational region $[-0.5, 0.5] \times [-0.5, 0.5]$ given as[12, 49, 50]

$$(\rho, u, v, p) = \begin{cases} (2, -0.5, 0.1sin(2\pi x), 2.5), & 0 \leq -0.25 \leq y \leq 0.5, \\ (1, 0.5, 0.1sin(2\pi x), 2.5), & otherwise. \end{cases} \tag{53}$$

We set all boundaries for this problem to periodic boundaries. Figure 22 shows the density contours for the various WENO schemes using 800×800 cells until $t = 1$ with 12 contours at [0.9,2.2]. We can see from the graph that the vortex structure of the WENO-SIF scheme is larger than that of the rest of the schemes. That shows the present scheme has a higher resolution than the rest of the schemes.

4.6. Computational time for 2-D problems

In this section, we will give the time consumed by various WENO methods to compute the 2D problem by using a desktop with an Intel i7-9700 CPU @ 3.00 GHz processor, and we list the results in Table 10. In the table, we will take the time taken by WENO-JS to get the relative time of the various WENO schemes. Among all WENO schemes, WENO-SIF uses the least amount of CPU time. Compared with the WENO-JS scheme, WENO-SIF saves at least about 20% of computation time. And the CPU time of WENO-SIF is even only 20% of WENO-PZ. Combining individual one- and two-dimensional problems, the WENO-SIF scheme provided in this paper has a higher computational efficiency than other WENO schemes.

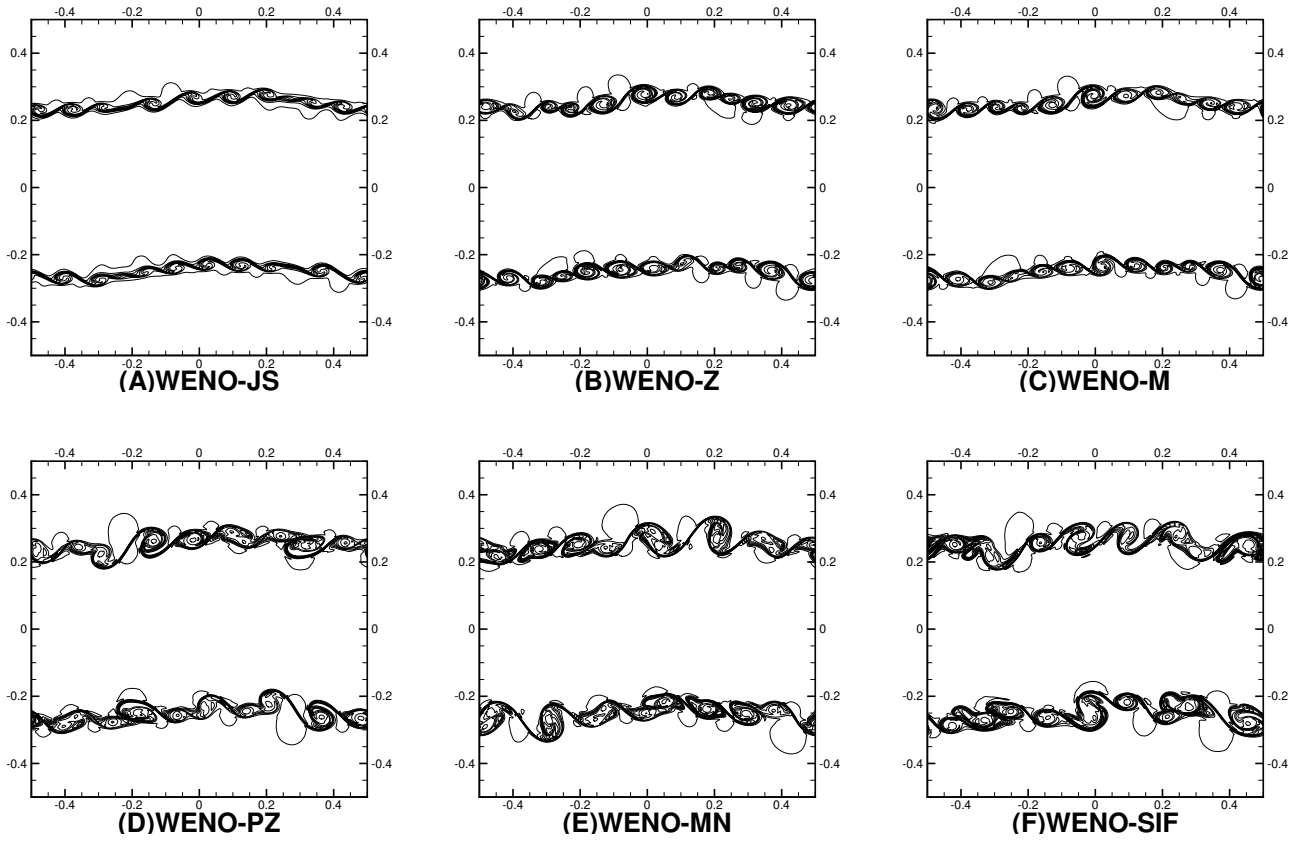

Fig. 22: Results of Forward-facing step problem: 45 density contours at $[0.9,\ 2.2]$ with 800×800 cells.

Table 10: CPU times for the 2-d problems with various WENO schemes.

Case	WENO-JS	WENO-Z	WENO-M	WENO-PZ	WENO-MN	WENO-SIF
2-D Riemann(case 1)	3059(1.00)	3502(1.14)	5031(1.64)	16080(5.26)	4380(1.43)	2319(0.76)
2-D Riemann(case 2)	7179(1.00)	7584(1.06)	10270(1.43)	26450(3.68)	9107(1.27)	5492(0.77)
Implosion	33440(1.00)	35690(1.07)	51430(1.54)	143300(4.29)	44210(1.32)	27060(0.81)
Double-Mach reflection	1361(1.00)	1491(1.10)	2194(1.61)	6305(4.63)	1918(1.41)	1021(0.75)
RT instability	10030(1.00)	10730(1.04)	14700(1.43)	38340(3.72)	12630(1.23)	7639(0.74)
Forward-facing step	10290(1.00)	10940(1.06)	15340(1.50)	44660(4.34)	13650(1.33)	8061(0.78)
Kelvin-Helmholtz instability	10610(1.00)	11430(1.08)	15560(1.47)	40220(3.79)	14130(1.33)	8897(0.84)

5. Conclusion

To improve the excitation capture capability of the third-order WENO-JS scheme and reduce the computational consumption, in this paper, we propose a new WENO scheme independent of the smooth factor. The weight functions of the WENO-SIF are the segmented linear functions of the ratio to the sub-stencil flux, which contain a tunable parameter λ. This function satisfies $\omega_0(0) = 1$ $(\omega_1(0) = 0)$ and $\omega_0(\infty) = 0$ $(\omega_1(\infty) = 1)$, which ensures the new present WENO scheme contains the ENO property. Numerical results show that the present WENO scheme can achieve the desired accuracy at high-order critical points and can further improve the resolution of WENO-JS by suppressing the numerical oscillations near the discontinuity points with a low extra computational cost.

Ethical Approval and Consent to participate

Not Applicable.

Consent for publication

Not applicable.

Availability of supporting data

The data sets supporting the results of this article are included within the article and its additional files.

Competing interests

The authors declare no competing interests.

Funding

This work is supported by Scientific Research Foundation of Hunan Provincial Education Department under Grant No.19C1766.

Authors' contributions

Shujiang Tang wrote the entire manuscript.

Acknowledgements

The author is grateful to the editors and reviewers for their constructive corrections and suggestions.

References

[1] A. Harten, High resolution schemes for hyperbolic conservation laws, J. Comput. Phys. 49 (1983) 357-393.

[2] X. D. Liu, S. Osher, T. Chan, Weighted essentially non-oscillatory schemes, J. Comput. Phys. 115 (1994) 200-212.

[3] G. S. Jiang, C. W. Shu, Efficient implementation of weighted ENO schemes, J. Comput. Phys. 126 (1996) 202-228.

[4] D. S. Balsara, C. W. Shu, Monotonicity Preserving Weighted Essentially Non-oscillatory Schemes with Increasingly High Order of Accuracy, J. Comput. Phys. 160 (2000) 405-452.

[5] J. Qiu, C. W. Shu, Hermite WENO schemes and their application as limiters for Runge-Kutta discontinuous Galerkin method: one-dimensional case, J. Comput. Phys. 193 (2003) 115-135.

[6] S. Rathan, G. N. Raju, A modified fifth-order WENO scheme for hyperbolic conservation laws, COMPUT. MATH. APPL. 75 (2018) 1531-1549.

[7] Z. Wang, J. Zhu, N. Zhao, A new fifth-order finite difference well-balanced multi-resolution WENO scheme for solving shallow water equations, COMPUT. MATH. APPL. 80 (2020) 1387-1404.

[8] A. K. Henrick, T.D. Aslam, J.M. Powers, Mapped weighted essentially non-oscillatory schemes: achieving optimal order near critical points, J. Comput. Phys. 207 (2005) 542-567.

[9] H. Feng, F. Hu, R. Wang, A new mapped weighted essentially non-oscillatory scheme, J. Sci. Comput. 51 (2012) 449-473.

[10] H. Feng, C. Huang, R. Wang, An improved mapped weighted essentially non-oscillatory scheme, Appl. Math. Comput. 232 (2014) 453-468.

[11] R. Wang, H. Feng, C. Huang, A new mapped weighted essentially non-oscillatory method using rational mapping function, J. Sci. Comput. 67 (2016) 540-580.

[12] U. S. Vevek, B. Zang, T. H. New, Adaptive mapping for high order WENO methods, J. Comput. Phys. 381 (2019) 162-188.

[13] Z. Hong, Z. Y. Ye, X. Z. Meng, A mapping-function-free WENO-M scheme with low computational cost, J. Comput. Phys. 405 (2020) 109145.

[14] F. X. Hu, High-order mapped WENO methods with improved efficiency, Computers & Fluids. 219 (2021) 104874.

[15] R. Li, W. Zhong, An efficient mapped WENO scheme using approximate constant mapping, arxiv.org, (2021) 2102.00231.

[16] Q. Li, P. Yan, X. Huang, L. Yang, F. Xu, Y. You, On Developing Piecewise Rational Mapping with Fine Regulation Capability for WENO Schemes, J. Sci. Comput. 88 (2021) 75.

[17] J. Zhu, J. Qiu, New Finite Diference Mapped WENO Schemes with Increasingly High Order of Accuracy, Communications on Applied Mathematics and Computation. 23 (2021).

[18] R. Borges, M. Carmona, B. Costa, W.S. Don, An improved weighted essentially non-oscillatory scheme for hyperbolic conservation laws, J Comput Phys 227 (2008) 3191-3211.

[19] M. Castro, B. Costa, WS Don. Wai, High order weighted essentially non-oscillatory WENO-Z schemes for hyperbolic conservation laws. J Comput Phys 230 (2011) 1766-1792.

[20] W. S. Don, R. Borges, Accuracy of the weighted essentially non-oscillatory conservative finite difference schemes. J Comput Phys 250 (2013) 347-372.

[21] S. Liu, Y. Shen, F. Zeng, Y. Ming, A new weighting method for improving the WENO-Z scheme. Int J Numer Meth Fl 87 (2018) 271-291.

[22] B. S. Wang, P. Li, Z. Gao, Don, W. S. Don, An improved fifth order alternative WENO-Z finite difference scheme for hyperbolic conservation laws, J. Comput. Phys. 374 (2018) 469-477.

[23] J. Peng, C. L. Zhai, G. X. Ni, H. Yong, Y. Q. Shen, An adaptive characteristic-wise reconstruction WENO-Z scheme for gas dynamic euler equations. Comput Fluids 179 (2019) 34-51.

[24] A. Baeza, R. Bürger, P. Mulet and D. Zoríio. On the Efficient Computation of Smoothness Indicators for a Class of WENO Reconstructions, J Sci Comput. 2019;80:1240-1263.

[25] A. Baeza, R. Bürger, P. Mulet and D. Zoríio. WENO reconstructions of unconditionally optimal high order, SIAM J NUMER ANAL, 2019;57:2760-2784.

[26] A. Baeza, R. Bürger, P. Mulet and D. Zoríio. An efficient third-order WENO scheme with unconditionally optimal accuracy, SIAM J Sci Comput.2020;42:1028-1051.

[27] F. X. Hu, A note on WENO-Z scheme. Appl Math Comput 396 (2021) 125886.

[28] M. Semplice, A. Coco, and G. Russo. Adaptive mesh refinement for hyperbolic systems based on third-order compact WENO reconstruction. Journal of Scientific Computing, 2016;66(2):692-724.

[29] M. Dumbser, W. Boscheri, M. Semplice, and G. Russo. Central weighted ENO schemes for hyperbolic conservation laws on fixed and moving unstructured meshes. SIAM J Sci Comput. 2017;39(6):2564-2591.

[30] Cravero, G. Puppo, M. Semplice, and G. Visconti. Cool WENO schemes. Computers and Fluids, 2018; 169:71-86.

[31] S. Rathan, N. R. Gande, A. A. Bhise, Simple smoothness indicator WENO-Z scheme for hyperbolic conservation laws, Appl. Numer. Math. 157 (2020) 255-275.

[32] C. Huang, L. Chen, A simple WENO-AO method for solving hyperbolic conservation laws, Appl. Math. Comput. 395 (2021) 125856.

[33] K. Yamaleevn, M. H. Carpenter. A systematic methodology for constructing high-order energystable WENO schemes. J Comput Phys. 228 (2009) 4248-4272.

[34] S. P. Liu, Y. Shen, B. Chen, F. J. Zeng. Novel local smoothness indicators for improving the third-order WENO scheme. Int J Numer Methods Fluids. 87 (2017) 51-69.

[35] X. S. Wu, Y. X. Zhao. A high-resolution hybrid scheme for hyperbolic conservation laws. Int J Numer Methods Fluids. 78 (201) 162-187.

[36] X. S. Wu, Y. X. Zhao. A new smoothness indicator for third-order WENO scheme. Int J Numer Methods Fluids. 81 (2016) 451-459.

[37] W. Z. Xu, W. G. Wu. Improvement of third-order WENO-Z scheme at critical points. Computers and Mathematics with Applications. 75 (2018) 3431-3452.

[38] Y. H. Wang, Y. L. Du, K. L. Zhao, L. Yuan. A low-dissipation third-order weighted essentially nonoscillatory scheme with a new reference smoothness indicator. Int J Numer Methods Fluids. 87 (2020) 1-23.

[39] G. Li, X. Li, P. Li, D. Cai, An improved third-order finite difference weighted essentially nonoscillatory scheme for hyperbolic conservation laws, Int J Numer Methods Fluids. 92 (2020) 1753-1777.

[40] X. Li, G. Li, and Y. Ge, Improvement of third-order finite difference WENO scheme at critical points, Int J Comput Fluid D. 34 (2020) 1-13.

[41] S. Tang, M. Li, Novel functional weights for improving the third-order WENO schemes, Int J Numer Methods Fluids. 93 (2021) 3131-3150.

[42] A. Kumar, B. Kaur, An Improvement of Third Order WENO Scheme for Convergence Rate at Critical Points with New Non-linear Weights, Differ Equat Dyn Sys, 28 (2020) 539-557.

[43] C. Li, Q. Guo, D. Sun, P. Liu, Improved third-order weighted essentially nonoscillatory schemes with new smoothness indicators, Int J Numer Methods Fluids. 93 (2021) 1-23.

[44] C. H. Kim, Y. Ha, H. Yang, J. Yoon, A third-order WENO scheme based on exponential polynomials for Hamilton-Jacobi equations, Applied Numerical Mathematics. 165 (2021) 167-183.

[45] S. Pirozzoli, On the spectral properties of shock-capturing schemes, J. Comput. Phys. 219 (2006) 489-497.

[46] P. Roe, Approximate Riemann Solvers, Parameter Vectors, and Difference Schemes, J. Comput. Phys. 43 (1981) 357-372.

[47] P. Woodward and P. Colella, The numerical simulation of two dimensional fluid flow with strong shocks, J. Comput. Phys. 54 (1984) 115-173.

[48] R. Liska, B. Wendroff, Comparison of several difffference schemes on 1D and 2D test problems for the Euler equations. SIAM J. Sci. Comput. 25 (2003) 995-1017.

[49] I. Christov, B. Popov, New non-oscillatory central schemes on unstructured triangulations for hyperbolic systems of conservation laws. J. Comput. Phys. 227 (2008) 5736-5757.

[50] P. D. Lax, Weak solutions of nonlinear hyperbolic equations and their numerical computation, Commun. Pure Appl. Math. 7 (1) (1954) 159-193.

[51] O. San, K. Kar, Numerical assessments of high-order accurate shock capturing schemes: Kelvin-Helmholtz type vortical structures in high-resolutions, Computers & Fluids. 89 (2014) 254-276.